PCCP

Accepted Manuscript

ROYAL SOCIETY OF CHEMISTRY

www.rsc.org/pccp

Effect of the components' interface on the synthesis of methanol over Cu/ZnO from CO_2/H_2: A microkinetic analysis based on DFT+*U* calculations

Qian-Lin Tang,* Wen-Tian Zou, Run-Kun Huang, Qi Wang and Xiao-Xuan Duan

Department of Applied Chemistry, School of Advanced Materials and Nanotechnology, Xidian University, No. 2 South Taibai Road, Xi'an 710071, People's Republic of China

E-mail: qltang@xidian.edu.cn (Q.-L. Tang). Tel.: (+86) 29-8189-1324. Fax: (+86) 29-8189-1371.

ABSTRACT: The elucidation of chemical reactions occurring on composite systems (*e.g.*, copper (Cu)/zincite (ZnO)) from first principles is a challenging task because of their very large sizes and complicated equilibrium geometries. By combining the density functional theory plus *U* (DFT+*U*) method with microkinetic modeling, the present study has investigated the role of the phase boundary in CO_2 hydrogenation to methanol over Cu/ZnO. The absence of hydrogenation locations created by the interface between the two catalyst components was revealed based on the calculated turnover frequency under realistic conditions, in which the importance of interfacial copper to provide spillover hydrogen for remote Cu(111) sites was stressed. Coupled with the fact that methanol production on the binary catalyst was recently believed to predominantly involve the bulk metallic surface, the spillover of interface hydrogen atoms onto Cu(111) facets facilitates the production process. The cooperative influence of the two different kinds of copper sites can be rationalized applying the Brönsted–Evans–Polanyi (BEP) relationship and allows us to find that the catalytic activity of ZnO-supported Cu catalysts is volcano type with decrease in the particle size. Our results here may have useful implications in future design of new Cu/ZnO-based materials for CO_2 transformation to methanol.

KEYWORDS: CO_2 hydrogenation, Cu-ZnO boundary, Hydrogen spillover, First-principles, Microkinetics

1. Introduction

The increase in the release of carbon dioxide (CO_2) into the atmosphere arguably poses the serious problems of global warming and climate change due to its greenhouse effect,[1-3] threatening the survival and development of humankind. Thus, in pursuit of a stable climate, there is an urgent need to develop efficient CO_2 capture and utilization systems.[3] One promising way to make progress in this direction is by using mixed metal and oxide materials as solid catalysts for the chemical fixation of CO_2 with hydrogen (H_2) to fuels and useful chemicals under applicable conditions.[4-14] For instance, it is now well established that the copper (Cu)/zincite (ZnO)-based catalysts display high activity and selectivity toward hydrogenation of CO_2 to methanol (H_3COH), the third-most large-scale chemical product, at pressures less than 100 bar and reaction temperatures in the range from 473 to 573 K.[6,11-13,15-18] Owing to the importance of the selective hydrogenation from both fundamental and practical points of view, a great deal of research efforts have been devoted worldwide to modifying the catalytic properties of the methanol synthesis catalysts.[14,18-27] The interaction of the Cu-metal deposits with the ZnO substrate has been ascertained to significantly influence catalytic performances for the formation of H_3COH.[6,10-12,19,22,28-32] Yet, in light of the high complexity of reactions taking place over composite catalysts, to achieve a clear understanding of this effect is a grand challenge in the community of heterogeneous catalysis.[3,24,33,34] Hence, to date, although both modern catalytic and surface science studies of Cu/ZnO-based CO_2 hydrogenation catalysts have been put in place over the past three decades,[3,19,31,35] some key issues in the catalytic system, as would be commented below, are still not fully clarified.[3,31] This lack of information impedes to a high extent the improvement of the production of methanol using Cu catalysts.

Ongoing debates regarding the Cu/ZnO catalysts themselves focus overwhelmingly on the identify of the active site and the role of the oxide support.[3,9,16,17,19,28,31,35-39] It was suggested in early reports[19,40-42] that the active centers are located on the sites of Cu^+ ions substituted in the matrix lattice. In sharp contrast, some other groups insisted that the Cu^0 and Cu^+ pair are essential to the formation of methanol from CO_2 and H_2 over the binary catalysts[17,23,28,38,43-47] and the Cu^+/Cu^0 ratio dictates the specific activity.[23,44] Apart from these two opinions, more experimental data[7,28,29,35,39,48-64] and

especially latest progress in theory[21,24,34,65] as well as in experimental work[11-14,18,22,25,34,66-68] concerning this reaction indicated that H_3COH generation involves exclusively the metallic instead of ionic copper. The existence of such an active phase in the catalysis system is clearly confirmed by the observations that the methanol formation rate relies on the amount of exposed Cu^0 atoms[11,12,14,22,23,26,32,66,67] and for a given feed gas composition and certain catalyst loadings, scales even linearly with the metallic copper surface area.[13,14,25,35,48,49,66] Consistently, density functional theory (DFT) calculations of CO_2 hydrogenation over Cu(111),[7,34,69,70] Cu(211),[34,65] unsupported Cu_{29} nanoparticles[7] and CeO_x/Cu(111)[24] predicted that these Cu substrates are rather active and selective for the methanol formation. Unsurprisingly, the ZnO was frequently speculated to serve in maintaining stable, high dispersion of Cu particles.[11,18,35,41,42,44,48,49,53,57,68] However, Deng and collaborators[64] noticed that too small catalyst particles impair H_3COH production by showing that the methanol yield increases with the increase of surface area of copper in the range of 5.8–28.8 m^2/g and then decreases above 28.8 m^2/g. The result was recently independently strengthened by another two groups: Karelovic et al.[14] and Natesakhawat et al.[66] It reflects that the activity of Cu/ZnO catalysts is not only related to Cu surface area but also to other causes.

Most probably the synergistic interaction between ZnO and Cu is also a key descriptor for the catalyst performance.[4,9-11,20,26,28,50,51,58,67,71-73] In this situation, different possibilities of the role of the metal oxide component in the CO_2 hydrogenation reaction were nevertheless put forward.[9,11-14,22,26,28,50,51,58,66,67,71-73] For example, it was found that the ZnO no longer simply acts as a reaction spectator but becomes a reservoir for atomic hydrogen, which promotes H spillover to Cu crystallites.[26,50,51] The oxide support was still envisaged to be able to induce the change in the morphology of Cu grains,[21,58,66] therefore resulting in larger numbers of open planes and edge/defect sites having coordinatively unsaturated Cu atoms which are typically more reactive than fully coordinated species.[66] More controversially, Frost[43] reported that a Sckottky junction effect between the Cu and ZnO partners may account for the enhanced activity of the supported transition-metal particles with reference to Cu alone, whereas Nakamura et al.[37,74-79] later pointed out that Cu-Zn alloying owing to the ZnO_x migration from the ZnO particles onto the Cu surface is responsible for the major promotional role of ZnO in the Cu/ZnO-based catalysts. The

latter argument is in complete accordance with proposals of some other research groups,[31,34,80,81] who claimed that surface alloys offer new catalytic sites for the synthesis reaction apart from metallic copper atoms. On the contrary, there are various evidences[3,4,6,9,10,14,17,20,22,27,28,30,32,46,64,71,72,82-85] that the particularly reactive sites created by the existence of ZnO are the oxide itself (such as oxide thin films and ZnO_x oxygen vacancies) and/or its boundary with copper, not the Cu-Zn alloy layer. In particular, the metal–oxide interface was shown experimentally[22,24,32,72] to beneficially affect the activity of the Cu particles and, very recently, this was also justified theoretically[24] by a DFT analysis of CO_2 hydrogenation on CeO_x/Cu(111).

Additionally, the accurate mechanism of the CO_2 to methanol process over Cu/ZnO catalysts remains quite divergent and unsettled in the literature.[3,20] It was long recognized that CO_2 can react directly with adsorbed H species to generate HCOO, followed by stepwise hydrogenation to give intermediate formic acid (HCOOH), dioxymethylene (H_2COO), hydroxymethoxy (H_2COOH), formaldehyde (H_2CO), methoxy (H_3CO) and the terminal product H_3COH.[7,30,44,47,50-54,56,58,61,63,71,72,74,75,77,85,86] Recently, first-principles calculations[34,65,70] revealed that HCOO hydrogenation proceeded via hydrogenation of one of the oxygen atoms of HCOO, not the carbon center. Other than the most accepted formate route, a few prior studies[19,24,40,70,82,83] supposed that the overall reaction network may also involve the reverse water-gas shift (RWGS) reaction ($CO_2 + H_2 \rightarrow CO + H_2O$), where CO_2 is first converted to CO which is then hydrogenated via formyl (HCO), H_2CO and H_3CO intermediates to form methanol. In conflict with this suggestion is the definitive work of Liu et al.[7] who, on the basis of experiment and DFT calculations, stated that the CO produced from the fast RWGS reaction does not undergo subsequent hydrogenation to H_3COH because of the poor stability of the surface HCO. On the other hand, Chorkendorff et al.,[55] Mims et al.[62] and Mei et al.[69] all asserted that the formation of methanol from CO_2 and H_2 mixtures on Cu cannot result from the simple hydrogenation of the formate species. Alternatively, using the periodic DFT method, the last group[69] proposed a novel carboxyl (HOCO)-mediated mechanism as the exclusive operative reaction path for methanol synthesis from CO_2 hydrogenation on Cu(111). The reactive surface species HOCO, which is formed by the reaction of CO_2 with adsorbed water, has to turn into hydroxymethylidyne (COH) through a dihydrocarbene (HOCOH) intermediate until several successive hydrogenations are

executed to yield H_3COH.

For methanol generation over Cu/ZnO catalysts, it is unanimously agreed that the rate determining step often appears on the surface of their metal components.[51,61,63,86] Hydrogenation of the HCOO adsorbate was perceived to limit the production of H_3COH in a series of papers[51,56,61,63,77,86] since it was identified to be the most abundant species on Cu by means of postreaction surface analysis such as X-ray photoelectron spectroscopy (XPS), temperature-programmed desorption (TPD) and Fourier transformation infrared spectroscopy (FTIR).[54,56,63] But kinetic experiments and modeling of the CO_2 hydrogenation on Cu(100)[20] and Cu/ZnO-based catalysts[54] evidently showed that hydrogenation of H_2COO functions as the rate-limiting step. In slight contradistinction to these statements, Liu and co-workers' work based on DFT calculations of Cu_{29} as well as Cu(111)[7] concluded that the whole reaction rates toward methanol are controlled by both HCOO and H_2COO hydrogenation steps. At variance, another FTIR study on Cu/ZnO from Edwards and Schrader[82] and recent first-principles microkinetic modeling on Cu(111) from Grabow and Mavrikakis[70] determined the recombination of H_3CO with surface atomic H to be rate-limiting for methanol formation. However, only two years later, using the BEEF-vdW functional, Studt and collaborators[65] suggested that in the sequence observed for CO_2 hydrogenation on Cu(211), the HCOOH + H channel is even more difficult than the H_3CO hydrogenation.

In view of the importance of the interplay between catalyst components and the existing discrepancies illustrated above, it would be highly desirable to at the atomic level know how the metal-oxide interface affects the synthesis of H_3COH via CO_2 hydrogenation over Cu/ZnO-based catalysts. Unfortunately, the published theoretical studies[7,34,65,69,70,85,87,88] concerning the surface chemistry of the complex systems revolved essentially around addressing the hydrogenation reaction either at isolated Cu phases[7,34,65,69,70] or on pure ZnO films.[85,88] To tackle this puzzle, in the present work the reaction process over a Cu strip supported on a completely actual ZnO surface was systematically explored utilizing a combination of *ab inito* DFT+*U* calculations and a mean-field treated microkinetic model. With a flat (extended) Cu(111) surface assumed to be a necessary, active site in Cu-based catalysts, a promotional effect of the Cu/ZnO interface on the catalytic activity toward methanol

synthesis was attained and analyzed. This effect was rationalized in terms of the hydrogen spillover mechanism from the boundary Cu atoms to their parent bulk surface, rather than in terms of the direct generation of a new active center by forming the components' interphase. The findings are likely to afford a valuable guide for the further development of more efficient Cu/ZnO methanol synthesis catalysts.

2. Computational methods and modeling

All electronic structure calculations were carried out with the Vienna *ab initio* simulation package (VASP)[89-93] using the generalized gradient approximation (GGA) parameterized by Perdew and Wang (PW91).[94] The valence-core electron interaction was treated within the projector augmented wave (PAW) formalism.[95,96] To account for the strong electron correlations in ZnO, the GGA+*U* scheme of Dudarev and co-workers[97] was applied to the zinc centers. The Hubbard *U*-like term ($U_{\text{eff}} = U - J$) was chosen to be 7.5 eV, which was formerly tested for consistency of the band structure with experiments.[98] Our recent work[99] has showed that this value does an excellent job of describing the surface work functions of the oxide. The Kohn–Sham (KS) equations were resolved employing a plane-wave basis set up to a kinetic energy cutoff of 400 eV. To speed up calculations, the electronic levels were broadened with a generalized Gaussian smearing technique[100] (width, 0.01 eV). The convergence criterion for the electronic self-consistent iteration was set to 10^{-5} eV per supercell. The quasi-Newton algorithm[101] was utilized for geometry optimization until the residual forces on all relaxed atoms disappeared within 0.03 eV/Å.

To characterize the geometrical microstructure of the catalytically active sites in composite systems (*e.g.* Cu/ZnO) at the atomic level of detail brings a formidable challenge to both experiment and theory,[34,102] in that the interactions of metal particles and the supports are of complex nature and result in many possible configurations for their phase interface.[3,11,21,34,102] At high-pressure CO_2 hydrogenation conditions, the ZnO component is well known to crystallize in a hexagonal wurtzite structure with space group $P6_3mc$;[103-105] among all relevant low-index ZnO facets, the $(10\bar{1}0)$ orientation has been predicted to be exposed preferentially on account of the lowest calculated surface energy.[106] Recent first-principles computations[99,107] indicate that this thermodynamically stable crystal plane emerges as the optimum binding site for

not only CO_2[99] but also Cu clusters to the support.[107] Besides, from the studies of Hansen and coworkers,[108] using in situ scanning tunneling microscopy (STM), the large majority of ZnO grains seem to be in intimate contact with the closed-packed Cu(111) surface with their $(10\bar{1}0)$ facets for a Cu/ZnO catalyst in various gas environments. For these reasons, we selected only the nonpolar surface as the support model. On the other hand, Nakamura et al.[44,79] documented that the ZnO_x-covered Cu(111) is a good model of Cu/ZnO catalysts for low-temperature methanol synthesis. In reality the active component (copper metal) of industrial $Cu/ZnO/Al_2O_3$ catalysts is nanodispersed in the ZnO matrix.[4,12,26,27,29,45,59,67,109] For example, another STM measurement of Rodriguez et al.[7,110] revealed that a triple-layer high Cu nanopyramid exhibiting a rather significant surface population of the Cu(111) face was even formed on the oxide surface. Motivated by the facts, we created the metal/oxide boundary by anchoring a three-layer thick close-packed strip, three atoms wide, of copper onto the top of a stoichiometric $ZnO(10\bar{1}0)$ film (c.f. Fig. 1). The resulting complementary interfaces I and II have analogous atomic arrangements by use of the shape of the Cu nanoparticle – that is, both of them merely comprise the lowest energy facets of the individual components, which makes the adsorbed strip sufficiently stable to resist disruption during the CO_2 hydrogenation process. It should be mentioned that similar approaches were introduced earlier to pinpoint the catalytic activities of Cu/ZrO_2,[33,111] Au/ZrO_2[112] and Au/TiO_2,[113,114] which was demonstrated to be successful in capturing the crucial chemistry of the metal-oxide perimeter interfaces.

The $ZnO(10\bar{1}0)$ was simulated by a repeating $p(4 \times 3)$ slab, with a surface unit cell of the size 12.65 Å × 15.24 Å containing six ZnO layers (Fig. 1b). A vacuum spacer of 18 Å was applied to avoid interactions between adsorbates and slab images. Such a large unit cell guarantees that the lattice mismatch between the optimized Cu strip and the supporting surface is small enough (1.49%) to prevent the buildup of considerable strain in the metal overlayer. The best geometry for the Cu strip on the oxide substrate was determined as follows: the system was first relaxed to arrive at an equilibrium state by running first-principles molecular dynamics (MD) with Nose thermostat at the investigated temperature of 523 K for 1 ps. Subsequently energy minimized snapshots extracted from the MD trajectories were singled out and optimized. The top

two layers of the oxide surface alongside with the Cu atoms and other possible adsorbates were allowed to move freely, keeping the rest of the ZnO atoms fixed at their bulk-truncated positions. Due to the large unit cell size, the first Brillouin zone was *k*-sampled at the Gamma point only. For the purpose of reference and comparison, a Cu(111) surface without ZnO was used to represent the metallic sites positioned far away from the support. To model the flat bulk surface, a four-layer slab with the outermost two layers relaxed was employed. A $p(4 \times 4)$ unit cell and a Monkhorst-Pack grid[115] of $(3 \times 3 \times 1)$ special *k* points were selected for the surface.

The adsorption/binding energy E_{ad} for an adsorbate X to a target substrate was calculated according to the equation

$$E_{ad} = E_{X/sub} - E_X - E_{sub},$$

where $E_{X/sub}$, E_X, and E_{sub} are the total energies of the surface covered with the X in the optimized geometry, the X in the gas phase, and the relaxed bare substrate, respectively. The free, isolated adsorbate was situated in a cubic vacuum box of 18 Å side length. With this definition, a negative E_{ad} reflects a release of energy or a favorable adsorption. Test calculations of selected adsorption energies have been conducted to substantiate the convergence with respect to the *k* point set and the number of oxide layers included. The climbing image nudged elastic band (CI-NEB) method[116,117] was applied to seek the minimum energy paths (MEPs) for chemical reactions. All the geometry structures were further checked by the harmonic vibrational analyses, yielding no imaginary frequencies for adsorbed intermediates and sole imaginary frequencies for transition states (TSs), respectively. During numerical vibrational calculations, the three-point finite difference approach was adopted with a step size of 0.015 Å for the displacements of the individual atoms along the Cartesian coordinates.

The activation energy, E_a, and the heat of reaction, E_r, for each elementary step were obtained in terms of the separately adsorbed species. The forward and reverse activation energies were defined as the total energy differences between the TS and the initial state (IS) and between the saddle point and the final state (FS), respectively. Without being specifically pointed out, the barrier henceforth refers to the barrier in

the forward direction. The reaction heat was taken as the difference in energy between the FS and the IS; in this way, a negative value of E_r characterizes an exothermic process on the surface. It is worthy to note that with the above GGA+*U* setup, the theoretical enthalpy change of $CO_2 + 3H_2 \rightarrow H_3COH + H_2O$ at 298 K and 5 MPa, -0.496 eV, agrees well with the experimental one, -0.424 eV.[16] Vibrational energy effects[118] were taken into account in the reported results. Rate constants *k* and preexponential factors A^0 for all the steps were evaluated applying transition state theory[119] and the statistical mechanics based on the Boltzmann distribution.[120] The explicit expressions used to compute the two kinds of kinetic parameters can be found in a very recent publication.[121] The title reaction was examined using a binary gas mixture of CO_2 and H_2 (H_2/CO_2 molar inlet ratio = 3) as the feedstock at 523 K and 5 MPa total pressure.[44] The absence of CO in the feeding gas is partially because metallic Cu, such as the Cu strip discussed here, was thought to be inactive for the methanol synthesis by CO hydrogenation on Cu/ZnO-based catalysts.[78] The GGA+*U*-derived reaction rate constants serve as initial input for the microkinetic model, in which the reactor was simulated following the ideal continuous stirred tank reactor (CSTR). The number of interfacial copper sites used was 3 μmol(sites)/g(catalyst), assuming that their concentration is only 1% of that of all Cu surface sites.[122] The complete set of time-dependent CSTR differential algebraic equations for each gas-phase and surface species was solved with the numerical methodology used in our previous articles.[111,121]

3. Results and discussion

3.1. Interface characteristics and adsorption of intermediates

The current work was initiated by examining atomic Cu deposition above anion and cation sites of the $ZnO(10\bar{1}0)$ surface. The copper monomer prefers to be located near a bridge position that a Zn atom would occupy if the slab grew by an extra single layer of ZnO, consistent with other DFT (Perdew, Burke, and Ernzerhof (PBE) functional[123]) slab studies.[107,124] Through our calculations, the corresponding adsorption energy is -1.52 eV at the PW91+*U* level, which is 0.26 eV less exothermic than the PW91 result (-1.78 eV). This is because the use of the conventional DFT approach, disregarding on-site Coulomb interaction strength, renders an

overestimation of the absolute binding energy values for molecular adsorption on the surface of strongly correlated transition-metal oxides.[125,126] It is intriguing to notice that the PW91-derived adsorption energy falls exactly between the PBE data from Wang et al. (-2.00 eV)[107] and Broqvist et al. (-1.69 to -1.66 eV),[124] and is clearly much closer to the latter result.[124] Our test calculations manifest that the value of 0.1 eV used in ref. 107 for the width of the Gaussian smearing function is simply too large to gives the fractional occupancies of the highest occupied KS orbitals for a gas phase Cu atom. This leads to a wrong total energy of the single, free atom, which was moreover found to be just 0.22 eV above the correct one. Naturally, the adsorption energy of monomeric Cu predicted by Wang and co-workers[107] is more negative and, thus, appears to be questionable.

More importantly, the PW91+*U* binding energy for the adatom at ZnO$(10\bar{1}0)$, we found, is in magnitude less than half of the calculated cohesive energy of bulk Cu (-3.48 eV in comparison with the experimental value of -3.49 eV[127]). It is therefore expected that the formation and growth of Cu clusters over the oxide surface are strongly favored thermochemically, which is congruent with the result of the aforementioned STM observation.[7,110] Our optimized Cu strip deposited onto ZnO is presented in Fig. 1c,d. The most important deformation of the strip structure upon adsorption was found for the second Cu layer with the breaking of all Cu-Cu bonds between the third and fourth atomic rows to form a less coordinated Cu edge in interface I (located at the position of the former row; see Fig. 1c) than in interface II. The lower coordination of the first interface can enhance its bonding capability; for example, the adsorption energy of atomic H at the interphase is 0.02 eV more stable compared to the second interface. Therefore, only the interface I was accounted for when searching for preferred configurations of the adsorption complexes. The Cu nanoparticle interacts with not only surface O anions but also adjacent Zn cations, with average Cu-O and Cu-Zn bond lengths of 2.05 and 2.70 Å, respectively. The computed energy of adsorption of the metal strip is -0.49 eV per Cu atom in contact with the underlying oxide. Besides, when decomposing the adsorption energy into interaction and deformation contributions according to the scheme described in ref. 99, the interaction energy of the Cu strip with the substrate partner ZnO was estimated to amount to only -0.73 eV per its bottom-layer atom. These reveal that the Cu phase is

not very strongly bound to the zinc oxide $(10\bar{1}0)$ nonpolar facet, in line with a temperature programmed reduction study of the interaction between Cu and ZnO nanoparticles by Tsang and collaborators.[10] The Bader charge analysis[128,129] of the present Cu/ZnO system indicates that the supported strip is positively charged by 1.05 |e| per unit cell, which is primarily ascribed to the donation of electrons from Cu to the neighboring lattice oxygen. As a consequence, the Cu atoms are not neutral but partially cationic in nature when in the vicinity of the components' boundary, which coincides with the experimental report of Kanai et al.[42]

Have established the Cu/ZnO boundary, it is possible to further exclude some of its exposed sites as the catalytic centers for CO_2 hydrogenation. The two reactants CO_2 and H_2 were calculated to only very weakly physisorb in the interface region, where the strongest binding energies of -0.06 and -0.10 eV were achieved at Cu-only sites, respectively. As a support to the PW91+*U* results, we mentioned that the ZnO component cannot operate as an adsorber and a source of CO_2 to methanol synthesis active centers, as evidenced by temperature-programmed reaction spectroscopy of CO_2 and H_2 on the $Cu/ZnO/Al_2O_3$ materials.[86] The lack of a chemisorbed CO_2 state on the oxide side of the Cu-ZnO boundary is attributed to saturation of the interfacial lattice oxygen with the deposited copper. Note that oxygen vacancies may be involved for the support under severe reducing conditions, and 1/4 of the oxygens missing has also been observed for a polar ZnO $(000\bar{1})$ surface.[32,130] With this in mind, we further scrutinized the case where one interfacial O atom was taken out of the current surface unit cell, thereby creating 1/4 coverage of oxygen vacancies at the interphase. Nevertheless, the so created point defect is not stable as during geometry optimization, the nearest-neighbor surface Zn atom drifted toward the corresponding O vacancy by 0.42 Å and eventually formed a Cu-Zn bond of 2.66 Å over the original vacant position with the metal strip. This is consistent with experimental observations[131,132] that Zn adspecies are present in the vicinity of the Cu-ZnO interface at highly reducing conditions. According to our computations, the hydrogenation of formic acid, which was recently proposed to be the rate-determining step in methanol synthesis on Cu,[47,65] has a slightly lower (by 0.07 eV) energy barrier in the Cu-Zn boundary compared to the unreduced boundary, indicating that the new interfacial site cannot substantially improve the kinetics of the synthesis process. Hence, on the Cu/ZnO

interface, we only addressed adsorption complexes at the defect-free sites.

For the same reason, also the ZnO location of the interface boundary is unstable for most of other reactive intermediates implicated in methanol synthesis. For instance, atomic hydrogen expresses a marked preference for the Cu part and its transport toward the oxide part via the interface O is energetically unfavorable. Rather, referred to the gaseous atom, the H adsorption energy at the Cu side amounts to -2.80 eV, which is 0.78 eV more exothermic than the value (-2.02 eV) acquired for the adatom that formed a hydroxyl group (OH) with an interfacial O atom. Kinetically, the adsorbed H species has to overcome a potential barrier of at least 1.18 eV to be displaced from the Cu strip to the support. From a combination of standard thermodynamic data[133,134] and DFT simulations, it was inferred that the chemical potential of 1/2 H_2 in the gas phase is 2.70 eV lower with respect to an isolated H atom under the reaction conditions of 523 K and 3.75 MPa partial pressure. Based on the above preliminary computations, the H_2 molecule thermodynamically favors to decompose at the interface Cu into two atomic H. As expected, the reaction only demands an activation barrier of 0.23 eV to be surmounted, which matches the general consensus that Cu particles supported over ZnO have high ability toward H_2 dissociation.[3,18,21,26,135] Due to the absence of a notable interaction with the materials' interface, CO_2 reacts most likely at the Cu strip via a so-called Eley-Rideal (ER) type mechanism,[136] in which the reactant molecule attacks the surface hydrogen atoms directly from the gas phase. In other words, once H_3COH can be produced by the CO_2 hydrogenation within the model boundary, the Cu atoms at the interface perimeter would perhaps offer the most reactive site for the production reaction.

Surface sites located directly at the edge of the interface Cu or in its immediate vicinity to the fifth row of copper atoms were found to be more active than other interfacial Cu sites; therefore, in the following only these former positions were considered when investigating the adsorption behaviors of the reaction intermediates between CO_2 + H_2 and methanol (see Fig. 1d for probable binding sites). The position preference, adsorption energy, and adsorbate-substrate bond lengths at equilibrium are summarized in Table 1. Fig. 2 illustrates the optimized adsorption configurations of all the surface species in the energetically most favorable states, whose internal geometrical parameters are represented on the figure as well. Aiming to get a

comprehensive insight into the potential energy surface (PES) of each adsorbate over the model Cu/ZnO catalyst interface, the current theoretically predicted adsorption energies for them on Cu(111) are also listed in Table 1 and are seen to be generally in excellent agreement with prior DFT determinations.[33,69,70]

The findings here display that for the Cu phase in the metal-oxide perimeter interface, adsorption is favored with H, O, hydroxyl (OH), CO, COH, monodentate HCOO (mono-HCOO), hydroxymethylene (HCOH), and H_3CO occupying threefold hollow positions, while other surface intermediates under scrutiny prefers lower coordination sites. Among all of them, the HCO, HCOO, HOCO, H_2CO, H_2COO, and H_2COOH are anchored to the metal strip preferentially through a bidentate linkage. Aside from the H_2 and CO_2 cases, the interactions of adsorbed H_2O, H_2CO, HCOOH, and H_3COH with the substrate were still calculated to be weak, larger than -0.55 eV. There exists a clear trend that the interfacial Cu further stabilizes all the reaction species as compared to its parent bulk Cu(111) surface by -0.60–-0.01 eV, suggesting that on supported Cu particles, surface adsorption prefers to take place at the interface with the ZnO matrix. Of course the improved stability by the strip can be interpreted, in part, as due to the lower coordination number (*CN*) of edge Cu atoms than that of the flat surface atoms (*CN* = 7 vs. 9), so that the extra dangling bonds induced by the edge make the interfacial Cu more active to molecular adsorption. In addition, the cationic characteristics of the supported Cu nanoparticle helps to further strengthen the electrostatic interplay of the substrate and surface adsorbates, which can be similarly explained as in the previous DFT work done on a Cu/ZrO_2 system.[111]

3.2. Reaction network for CO_2 hydrogenation to methanol

Now, starting from CO_2 and adsorbed atomic H, we explored all potential reaction routes on the Cu side of the Cu/ZnO interface that may give rise to the final desired H_3COH product, which are named here as the HCOO path, the HOCO path, and the CO path according to the way that the first hydrogen adatom is added to the incoming CO_2. On the basis of our extensive DFT+*U* calculations, the PESs of the methanol synthesis via the three distinct mechanisms were identified and mapped out in Fig. 3-5, respectively. Additionally, Table 2 collects the vibrational frequency, reaction energy, activation barrier, and preexponential factor, as well as the calculated forward and

reverse rate constants, at the temperature mentioned above for each one of the elementary steps considered in the present study. Briefly, they were described in what follows.

HCOO path. The route, which is given in Fig. 3, is initiated by the attack of the carbon atom on the gaseous CO_2 molecule to the H* atom at a pseudo-hcp (phcp) hollow site of the Cu strip via a TS (TS2) to generate mono-HCOO* (a species' name followed by * denotes the species adsorbed on a vacant interface site *). In the TS2, the adatom H* sits on the bridge site exactly between two Cu atoms of the fifth row (bri3 in Fig. 1d) at distances of 1.73 Å. The H–C contact arrives at 1.56 Å, versus 1.11 Å for the FS. This process is moderately uphill, with a reaction heat of +0.49 eV and an activation barrier of 0.79 eV. The binding mode of the formate intermediate is metastable and quickly rearranges to its more stable bidentate counterpart bi-HCOO*, the barrier of which is just 0.10 eV high. The reaction channel is bifurcated at the bi-HCOO* point until getting H_2COOH*. Here at first inspection, two possibilities are implicated: one commences from H_2COO*, which is formed by further hydrogenation on the C center of bi-HCOO*; the other goes via HCOOH* that is generated by H* addition to an oxygen location of bi-HCOO*. However, actually, the first branch has to be ruled out thanks to a fairly sizable barrier of 2.10 eV to the H_2COO* formation. Alternatively, H_2COOH* is energetically available for the second branch. Its constituent elementary steps bi-HCOO* + H* $\rightarrow$ HCOOH* + * and HCOOH* + H* $\rightarrow$ H_2COOH* + *, although endothermic, overcome lower barriers (less than 1.30 eV) in comparison with the bi-HCOO* to H_2COO* reaction. The TS (TS7) of the HCOOH* + H* $\rightarrow$ H_2COOH* + * step features an sp^3-like carbon and a forming H-C bond of 1.41 Å. It is interestingly noticed that the corresponding activation energy is roughly 1.5-fold larger than the HCOOH* desorption energy. The interfering desorption effect implies that the forward hydrogenation reaction of adsorbed formic acid, if any at all, is still a difficult one.

The H_2COOH* species once formed would decompose into H_2CO* and OH*. Tilting the O–C–O skeleton toward the underlying Cu substrate launches this reaction. In the TS (TS8), the leaving OH group is in a bridge position (bri2 in Fig. 1d), whereas the remaining H_2CO* fragment ends up on an edge Cu atom through its O end. Relative to that in the IS, the activated C–O bond is stretched by ~1 Å to 2.44 Å, suggesting

that the bond is already cleaved. Upon coadsorption, H_2CO^* and OH*, the products of H_2COOH^* dissociation, attract each other by -0.07 eV. The MEP calculation reveals that this is a very facile step, with a low barrier height of 0.28 eV. The reaction of the yielded H_2CO^* with H* to afford an adsorbed H_3CO species was calculated to be exothermic (E_r = -0.35 eV) with an activation energy of 0.48 eV. Moreover, the barrier is just somewhat greater (0.1 eV) than that of H_2CO^* desorption from the materials' interface. Consequently, H_3CO^* formation could compete with the desorption of formaldehyde for H_2CO^* consumption. At last, H_3COH^* is produced either through the direct hydrogenation of H_3CO^* ($H_3CO^* + H^* \rightarrow H_3COH^* + *$) or, taking into account that water is a reaction product of methanol synthesis, through a hydrogen transfer from H_2O^* to H_3CO^* ($H_3CO^* + H_2O^* \rightarrow H_3COH^* + OH^*$). As far as energetics are concerned alone, the latter pathway wins over the former. With the assistance of the surrounding H_2O^* molecule, the H_3CO^* to H_3COH^* process is nearly spontaneous (E_a = 0.02 eV). Nevertheless, the barrier for this proton transfer event is increased up to as high as 1.34 eV when the vicinity of the reactive site is free of adsorbed water.

HOCO path. Similarly to the above mechanism, this pathway (Fig. 4) also begins with the direct interaction of gas phase CO_2 with surface atomic H* but in a different fashion–through one O end instead of the central C atom, which produces a *trans*-carboxyl (*trans*-HOCO*) species. The length for the making O–H bond at the TS (TS13) measures 1.41 Å. The reaction profile is characterized by a large endothermicity of 0.70 eV and high energy barrier of 1.43 eV. Thus, it seems that such a hydrogenation step, while not impossible, is not easy to conduct. The CO_2 molecule may also accept a proton from the interface H_2O^* to liberate the *trans*-HOCO*. For the TS (TS14), the nascent O–H bond distance is 1.24 Å, 0.21 Å longer than the value in the final, coadsorbed state *trans*-HOCO*···OH*. The hydrogen transfer path is slightly endothermic (E_r = 0.24 eV), and its activation energy barrier, 0.27 eV, is significantly smaller than that of direct CO_2 hydrogenation, $CO_2 + H^* \rightarrow$ *trans*-HOCO*. Hence, in the presence of nearby water, CO_2 conversion to *trans*-HOCO* energetically tends to take place through the intermolecular proton transfer mechanism. Subsequently, the *trans*-HOCO* intermediate undergoes a structural transformation to the essentially isoenergetic *cis*-HOCO* conformer, which is activated by as low as 0.40 eV.

At the stage of the *cis*-carboxyl adsorbate, the course of the reaction diverges into two paths towards the adsorbed product species, H_3COH*. Firstly, the *cis*-HOCO* continues to react with another H* to generate two possible intermediates, i.e. HOCOH* and HCOOH*. The HOCOH* formation reaction is highly endothermic (ΔE_r = 0.79 eV) with a barrier height of 1.07 eV, whereas the parallel hydrogenation of *cis*-HOCO at the carbon atom is virtually thermoneutral (E_r = -0.06 eV) with a somewhat lower barrier of 0.97 eV. In the transition states of the two elementary steps (TS16 and TS17), the reactive H* adatoms were both approaching a bri2 bridge location, with the newly forming H–O and H–C bond lengths, respectively, of 1.39 and 1.40 Å. On one hand, the generated HOCOH* species experiences a high barrier of 1.29 eV to decomposition into COH* and OH*, even though the reaction is almost thermoneutral (ΔE_r = 0.06 eV). As soon as the TS (TS18) is reached, the HO–COH bond is broken over an fcc-type site (pfcc) with the OH* and COH* fragments lying on distorted edge-bridge (bri1) and phcp positions, respectively. The dissociating C–O distance is already 2.02 Å long. Next, the COH* moiety is progressively hydrogenated to release methanol, which walks along the route COH* $\rightarrow$ HCOH* $\rightarrow$ H_2COH* $\rightarrow$ H_3COH* $\rightarrow$ H_3COH. The barrier heights of 1.02, 0.87, 0.85, and 0.36 eV were obtained in turn for the four steps. On the other hand, the surface HCOOH* also changes into H_3COH following the sequence as in the hereinbefore discussed HCOO path. As apparently shown in Fig. 4, the present conversion process is in energy more feasible for forming methanol than the route starting from HOCOH*.

CO path. The reaction coordinate for the current path is depicted in Fig. 5. The channel network implicates the creation of a CO* complex, followed by sequential hydrogenation of the surface species to H_3COH. At first sight, the adsorbed CO* presumably originates directly from the splitting of the CO_2 reactant through a late-type TS (TS22). In the TS22, the dissociating O atom is shifted to a bri3 bridge site, while the forming CO* intermediate is positioned on an edge Cu atom. As a result, the distance for the cleaving C–O bond is substantially extended to 1.93 Å from the original bond length of 1.18 Å. The energy barrier was computed to be 1.00 eV. This value is very close to the experimental data that vary between 0.76 and 0.99 eV for a fresh $Cu/ZnO/Al_2O_3$ catalyst reduced in H_2 at 513 K.[137] The close agreement with practice further verifies the adequacy of the Cu/ZnO model adopted here, giving us confidence in the results. An alternative path for CO* evolution at the present

interfacial Cu is offered by the decomposition of surface carboxyl. Compared with the slightly endothermic CO_2 dissociation, the *cis*-HOCO* + * → CO* + OH* step is moderately exothermic by 0.66 eV with a lower, by 0.56 eV, barrier.

The reaction pathway again bifurcates from CO* whose initial reaction with an H* adatom would lead to either COH* or HCO*. In fact, the route proceeding through three consecutive hydrogenation steps of the COH* intermediate can be precluded for H_3COH synthesis as hydroxymethylidyne formation from CO* + H* was found to be kinetically unlikely (E_a = 2.17 eV). Such a prohibitive barrier is predominantly associated with the weak interaction between the CO* and H* at the TS (TS24). The second path to yield methanol is via HCO* hydrogenation and, as displayed in Fig. 5, it is energetically more efficient than the first one. As for the current H_3COH generation route, the maximum barrier of 1.44 eV arises at the step CO* + H* → HCO* + *. It is critical to note that the value lies 0.22 eV above the barrier height of CO* desorption. Furthermore, the forward reaction of the resultant HCO* possesses a barrier (0.84 eV) that is around three times the barrier (0.27) of its backward reaction, which leads to the conclusion that the adsorbate is unstable and preferentially decomposes back into CO* and atomic H*. Accordingly, it is evident that the majority of the interface CO* species has a tendency to desorb from the copper strip, rather than be hydrogenated to HCO*. And certainly, so long as the reaction of HCO* + H* to H_2CO* occurs, the H_2CO* intermediate so obtained could be further converted to H_3COH* along the path previously depicted.

In the end, residual surface O* and OH* are removed from the components' boundary in the form of water, as represented in Fig. 3-5, to complete the whole catalytic cycle. Firstly, the recombination of the O* with an H* atom again resulted in the OH* intermediate, which is basically thermoneutral (ΔE_r = -0.07 eV) but with a comparatively high barrier of 1.08 eV. At the TS (TS27), both the atomic species are located at adjacent hollow sites above the Cu strip and are separated by 1.50 Å. In the FS, the formed OH* group occupies the phcp adsorption position of the original O* in a vertical orientation via three O–Cu bonds of averaged length 2.01 Å. Secondly, a weakly bonded H_2O* on top of the edge Cu atom can be produced by the direct hydrogenation (OH* + H* → H_2O* + *) or disproportionation of the adsorbed OH (2OH* → H_2O* + O*). The latter step is also a proton transfer. The making and

cleaving H–O bond distances in the TS (TS28) are respectively equal to 1.34 and 1.12 Å. The height of the barrier was predicted to be only 0.26 eV, and the endothermic heat, with respect to the coadsorbed H_2O^* and O*, is 0.14 eV. The two values are smaller than those (1.28 eV and 0.34 eV) of the OH* + H* reaction. On the energetic grounds, the disproportionation step is favored over the recombination reaction of the species OH* and H*.

It can be seen from Table 2 that with regard to the entire reaction network of CO_2 hydrogenation at the Cu site of the Cu/ZnO interface boundary, the preexponential factors are at least five orders of magnitude slower for the elementary steps with participation of a gas-phase H_2 or CO_2 molecule compared to other steps. The difference stems mainly from the large entropies *S* of the two molecules at elevated temperatures.[111,118] As found in standard thermochemical databases,[133,134] for 1 mol H_2 at (523 K,1 bar), the *S* value is increased relative to that at 0 K by 147.05 J/mol K, whereas it is 236.92 J/mol K for CO_2. Obviously a greater increase in entropy over the same temperature change appears in the latter species, which again renders the preexponential factors of the reactions of CO_2 much smaller than that of H_2 dissociation. As a consequence, and inasmuch as the dry CO_2 always experiences a relatively high barrier to reaction regardless of breaking or creating a chemical bond, the calculated reaction rate constants do not exceed 2.62×10^{-2} s^{-1}, which is much lower than the ones found for all the following steps along the corresponding possible methanol synthesis routes. Such small rate constants imply that the CO_2 activation by the interface Cu substrate is very difficult to perform and thus acts as a bottleneck step in the synthesis reaction. It must be emphasized that comparing individual rate constants might be misleading and can not ensure a reliable estimation of each pathway contribution.[121] Instead, microkinetic analysis in the next section will show the precise reaction kinetics of the complex interface catalysis.

3.3. Role of the interfacial Cu in promoting methanol formation

In order to quantitatively assess the power of the Cu/ZnO interface to catalyze CO_2 hydrogenation into H_3COH, the microkinetic model in the context of a mean field approximation was built on the basis of all the HCOO-, HOCO- and CO-mediated methanol synthesis mechanisms already described, including a total of 38 elementary

reactions tabulated in Table 2. It is important to note that interface H atoms would quite likely diffuse to the Cu(111) facet (assigned as *′) in remote distance from the zinc oxide with a low barrier of 0.42 eV (see the H* + *′ → H*′ + * step in Table 2). Furthermore, the diffusion rate constant at 523 K, 9.77×10^8 s^{-1}, is at least 10^6 times larger than for elementary steps involving CO_2. Maybe the hydrogen transport also takes place from the interface boundary to the catalyst support as its rate constant is only somewhat slower than that of the energetically permitted proton-transfer reaction of CO_2 and H_2O*. Therefore, the free migrations of H adatoms between different sites were naturally incorporated into the microkinetic modeling. Following the catalytic theoretical work of Grabow and Mavrikakis,[70] the initial surface coverages of the H adatoms and the free sites on the parent bulk Cu(111) facet were set to 0.15 and 0.57 ML, respectively. The forward and reverse rate constants of each constituent elementary reaction in the overall synthesis process, as calculated within the DFT+*U* framework, were employed for defining the developed model. No assumptions as to the biased mechanism and the rate-determining step were made. The simulated kinetic results were achieved when the steady state was reached. It is worth mentioning in passing that at typical methanol synthesis temperatures (~500 K), Grabow and Mavrikakis[70] have demonstrated the adsorbates on $Cu/ZnO/Al_2O_3$ to be highly disordered and diffusion limitations to be ignorable, both of which satisfy the underlying assumptions of mean-field microkinetic models. Therefore, our microkinetic model is justified as sufficiently accurate for the present purpose.

The equilibrium interface coverage of all pertinent adsorbates from microkinetic simulation is presented in Table 3. Inspection of Table 3 suggests that most of the interface region of the Cu strip was covered by H*. Second to the atomic species, vacant sites make up a certain proportion of the surface. The concentration of other intermediates is less than 10^{-3} ML. Given that, as demonstrated by our first-principles computations, CO_2 binds to the Cu/ZnO boundary very weakly or not at all, it is not surprising to predict a limited interface coverage for each carbon dioxide-derived species. Interestingly, we found that water has an extremely small surface concentration of $\theta_{H2O*} = 3.33 \times 10^{-19}$ ML under the used methanol synthesis conditions. Therefore, the hydrogen donation of H_2O* toward a neighboring intermediate even without a high barrier is kinetically inhibited by the absence of abundant interfacial water. Taking the conversion of CO_2 to *trans*-HOCO* as the

example, the CO_2 + H_2O* indeed raised the rate constant of *trans*-HOCO* formation by a factor of 10^{10} relative to the CO_2 + H* through improving its activation barrier. On the other hand, the coverage of adsorbed water is nevertheless 18 orders of magnitude lower than the one of H*. As a consequence, judging from the rate equation $r = k\theta_{H2O*}\theta_{CO2*}$, the reaction with H_2O* is not accelerated but decelerated approximately 10^8-fold. More importantly, H_3COH* is a negligible interface species with the coverage of 2.25×10^{-21} ML. Its coverage directly associates with the yield of the aspired gas product H_3COH.

From Table 4, which lists the theoretical turnover frequencies (TOFs) for the final products, it is seen that H_3COH formation via any hydrogenation routes of CO_2 is not viable on the interfacial copper sites, with a vanishingly small TOF value being 8.01×10^{-16} s^{-1}. Intriguingly, the reason for this is not that the Cu side was "poisoned" by H whose steady state coverage is close to 1 ML, but simply that all the early steps of CO_2 hydrogenation therein are not facile. If the diffusion of hydrogen to other sites was assumed to be irreversible, most of the interface copper zone would be empty and no methanol could still be generated for the strip. We further added two extra H atoms per unit cell as the preadsorbed spectator species in the vicinity of the reactive site to simulate the influence of a high interfacial hydrogen coverage on the slow kinetics of the CO_2 to HCOO* conversion. As a result, co-adsorbed hydrogen hardly affects the formate production by looking at an increase of the hydrogenation barrier relative to that of the clean substrate by only 0.01 eV. Our finding is in keeping with the work by Fujitani and co-workers,[74,78] who observed that the metal-oxide interface boundary cannot create catalytically active locations for the hydrogenation reaction. However, it is not the case for the Cu/ZrO_2 interface, which was shown to be highly reactive toward fixing CO_2 into methanol.[33,138,139] The activity difference can be explained by the fact that, as opposed to the former boundary, the latter consists of coordinatively unsaturated lattice oxygen that is required to facilitate efficient activation of CO_2.[24,33] On the basis of the current modeling, none of the side reactions to yield CO, H_2CO or HCOOH can as well proceed in the boundary between the metal and the ZnO due to their TOFs of at most 3.60×10^{-6} s^{-1}.

Although CO_2 hydrogenation in the Cu regions far from the interface was not explicitly considered within the present model due to their exceedingly large sizes, the

results here provide indirect support for the gradually growing proof that metallic copper is the active ingredient of Cu/ZnO catalysts in the hydrogenation of CO_2 to methanol.[7,11-14,22,25,28,29,35,39,48-62,65-70] A recent example is the effort of Grabow and Mavrikakis,[70] reporting that the hydrogenation reaction using a commercial $Cu/ZnO/Al_2O_3$ catalyst most likely takes place at the Cu(111) locus. With this in mind, while investigating the Cu/ZnO interface, we naturally compared it with the pure, extended metal facet. The present computations indicate that H_2 dissociative adsorption is greatly enhanced on the copper atoms that are in proximity to the oxide support: the activation energy is reduced by 0.15 eV relative to that of the Cu(111) case, increasing the rate constant by a factor of approximately 30. This agrees well with characterization of H_2-TPD,[18,26] which revealed that the ZnO improved the adsorption/activation of H_2 on Cu catalysts. The microkinetic model predicted that the coverage of atomic H on the Cu crystal (111) plane was increased by 20% to 0.18 ML when ZnO is present in the catalyst. That is, a substantial amount of dissociated hydrogen atoms would migrate off the interface Cu onto its parent bulk surface. In addition, our theoretical prediction also demonstrated that the accumulated hydrogen occupied more than 1/2 of the surface of the support and can be readily returned back to the interface with a significant rate constant of 1.19×10^4 s^{-1}. Therefore, it is easy to envisage that Cu particles exhibit a dramatic enhancement of activity in presence of ZnO, as spillover H assists in the conversion of an intermediate to a more fully hydrogenated adsorbed species occurring on the Cu(111) domain and/or other catalyst reactive sites. It may also be a possible cause why in the prior XPS studies of the CO_2 hydrogenation over clean Cu(111) and Zn-deposited Cu(111) by Fujitani et al.,[44,84] the new Cu^+-O-Zn sites created between ZnO_x and the single crystal surface during the reaction were observed to improve appreciably the TOF of methanol formation at copper. Overall speaking, the Cu/ZnO boundary as well as the support plays the role of storing surface hydrogen atoms and supplying these atoms to hydrogenation active sites by spillover. It is encouraging to note that in experiment,[4,18,26,50,51,72,82,139] a little attention was already paid to the importance of hydrogen spillover during methanol synthesis on Cu based composite catalysts.

The existence of the significant difference in chemistry between the Cu/ZnO interface and the reference Cu(111) surface may be traced back to the stronger affinity of interfacial Cu cations for surface intermediates, as elucidated earlier from section 3.1.

For this reason, considering the net change of molecular number before and after reaction, the thermodynamic driving force is lowered for an elementary recombination step and raised for an elementary splitting step upon moving from Cu(111) to the interface Cu. According to the well-known Brönsted–Evans–Polanyi (BEP) rule in catalysis,[140,141] the former kind of reaction is expected to be kinetically more favorable on the bulk Cu surface, while the latter one would be faster at the components' interface. The hydrogenation of H_3CO^* to H_3COH^* ($H_3CO^* + H^* \rightarrow H_3COH^* + *$) was chosen as an example because the reaction channel was recently regarded as the rate-controlling step of methanol synthesis with CO_2/H_2 over Cu catalysts.[70] Based on our calculations, H_3CO^* hydrogenation on the Cu(111) facet is 0.31 eV less endothermic than on the interfacial Cu atoms of the model Cu/ZnO system and thus the corresponding barrier is noticeably lower (1.04 vs. 1.34 eV). In practice the vast majority of the elementary steps in various methanol synthesis routes are categorized as recombination reactions. Hence, taking both thermodynamic and kinetic considerations, one can anticipate that the regioselectivity of the CO_2 hydrogenation to methanol prefers the metallic Cu site to the slightly charged interface of a Cu/ZnO catalyst. Nevertheless, the components' interface, or rather its Cu side, is not a spectator location for the reaction but actually serves to boost H_2 dissociation and, as already mentioned, store atomic hydrogen needed to hydrogenate reactive species. The result signifies that a dynamic active center may provide an essential structural prerequisite for highly catalytically active Cu/ZnO materials. In fact, published experimental[47,66,67] and theoretical studies[34,58,70] of this sort of catalysts have shown that relative distribution of different Cu facets notably affects substrate selectivity and product formation.

The synergistic effect between the interface Cu as well as the Cu(111) orientation in Cu/ZnO for CO_2 hydrogenation shows that methanol generation over the catalyst may be dominated by the size of Cu grains. With the greater activity at the flat surface caused by the above determined H spillover, the whole generation rate is envisioned to increase with the decrease of Cu particle size since small Cu particles will be constituted by more (111) facets and also give rise to larger Cu/ZnO boundary population which offers more spillover hydrogen atoms for hydrogenation steps. However, catalyst particles cannot be excessively small, otherwise the number of exposed active sites such as Cu(111) assumed here will reduce, which in turn will

lower the activity of CO_2 hydrogenation. Phrased differently, the supported Cu has optimal activity at appropriate particle sizes only, perhaps giving a clue for improving methanol synthesis catalysts. The finding supports the experimental observations,[64,76] in which Deng et al.[64] and Fujitani and Nakamura[76] points to a volcano-like activity dependence of Cu/ZnO catalysts on the surface area of metallic copper. Consistently, the latest catalytic activity measurements and X-ray diffraction data by Karelovic and coworkers[14] also confirmed that methanol synthesis from CO_2 is structure sensitive with too small Cu particles demonstrating very poor selectivity to the target product at constant CO_2 conversion. The results presented in the current paper provide an explanation from the atomic level, emphasizing the crucial role of interfacial Cu atoms.

4. Conclusions

To recap, this work presents the first detailed study on the working mechanism of a metal/oxide interface in a complex catalytic system by performing *ab inito* DFT+*U* calculations coupled with microkinetic simulation, that is, Cu supported on ZnO for CO_2 hydrogenation to methanol. The main conclusions are outlined as follows.

Using extensive first-principles calculations, it was found that the ZnO support does not directly take part in the methanol synthesis since its interface with copper is short of undercoordinated lattice O atoms that contribute to stabilization and activation of intermediates on the oxide side. Hence, only at the Cu site of the Cu/ZnO model interface were all pathways proposed in the literature for H_3COH formation over Cu catalysts (namely, HCOO-, HOCO- and CO-mediated reaction mechanisms) analyzed, making it possible to give a full picture of CO_2 hydrogenation chemistry therein. Invoking microkinetic principles based on theoretically predicted rate constants, we determined that these reaction pathways considered fail to produce methanol with a negligible total TOF of 8.01×10^{-16} s^{-1}. This has something to do with the weak interaction of CO_2 with the interfacial Cu. Still, with the exception of H adatoms, no any unwanted byproducts such as CO, H_2CO, and HCOOH were generated at the metal-oxide interface boundary.

By assuming that a metallic Cu(111) substrate is the active component of a Cu/ZnO

methanol synthesis catalyst, our modeling results evidently indicate that a large amount of hydrogen atoms produced at the interfacial Cu phase were spilled onto its parent bulk surface Cu(111). The diffusion event gives an extra source of atomic hydrogen required for the hydrogenation steps proceeding on Cu(111) (and other active centers without interaction with ZnO), which consequently promotes the entire process of CO_2 hydrogenation. On the other hand, hydrogen adatoms sterically occupies nearly all the interfacial Cu atoms and more than 1/2 of the ZnO surface; thus, the metal-oxide boundary as well as the catalyst support also functions as a reservoir for spillover hydrogen. According to the synergy of the components' interface and bulk Cu facets, the Cu/ZnO composite materials exhibit a volcano-type relationship of the catalytic activity in methanol synthesis to the particle size of supported Cu, in accord with prior experimental studies. The current findings, we think, can render some clues to the development of novel Cu/ZnO-based catalysts that will improve the CO_2 hydrogenation performance.

Acknowledgments

The National Natural Science Foundation of China is acknowledged for its financial support of the project under Contract No. 21003098 and the Fundamental Research Funds for the Central Universities of China for support under Contract No. JB141403. The authors are sincerely grateful to Z.-L. Pan for his assistance in the data analyses.

References

1 C.-S. Song, *Catal. Today*, 2006, **115**, 2-32.

2 K. M. K. Yu, C. M. Y. Yeung, and S. C. Tsang, *J. Am. Chem. Soc.*, 2007, **129**, 6360-6361.

3 W. Wang, S.-P. Wang, X.-B. Ma, and J.-L. Gong, *Chem. Soc. Rev.*, 2011, **40**, 3703-3727.

4 L.-Y. Ma, T. Tran, and M. S. Wainwright, *Top. Catal.*, 2003, **22**, 287-293.

5 X.-L. Liang, X. Dong, G.-D. Lin, and H.-B. Zhang, *Appl. Catal. B-Environ.*, 2009, **88**, 315-322.

6 Y. Ma, Q. Sun, D. Wu, W.-H. Fan, Y.-L. Zhang, and J.-F. Deng, *Appl. Catal. A: Gen.*, 1998, **171**, 45-55.

7 Y.-X. Yang, J. Evans, J. A. Rodriguez, M. G. White, and P. Liu, *Phys. Chem. Chem. Phys.*, 2010, **12**, 9909-9917.

8 R.-G. Zhang, H.-Y. Liu, B.-J. Wang, and L.-X. Ling, *Appl. Catal. B-Environ.*, 2012, **126**, 108-120.

9 F. C. Meunier, *Angew. Chem. Int. Ed.*, 2011, **50**, 4053-4054.

10 F.-L. Liao, Y.-Q. Huang, J.-W. Ge, W.-R. Zheng, K. Tedsree, P. Collier, X.-L. Hong, and S. C. Tsang, *Angew. Chem. Int. Ed.*, 2011, **50**, 2162-2165.

11 S. Zander, E. L. Kunkes, M. E. Schuster, J. Schumann, G. Weinberg, D. Teschner, N. Jacobsen, R. Schlögl, and M. Behrens, *Angew. Chem. Int. Ed.*, 2013, **52**, 6536-6540.

12 H. Ahouari, A. Soualah, A. L. Valant, L. Pinard, P. Magnoux, and Y. Pouilloux, *Reac. Kinet. Mech. Cat.*, 2013, **110**, 131-145.

13 K. C. Waugh, *Catal. Lett.*, 2012, **142**, 1153-1166.

14 A. Karelovic, A. Bargibant, C. Fernández, and P. Ruiz, *Catal. Today*, 2012, **197**, 109-118.

15 M. Saito and K. Murata, *Catal. Surv. Asia*, 2004, **8**, 285-294.

16 J. Wambach, A. Baiker, and A. Wokaun, *Phys. Chem. Chem. Phys.*, 1999, **1**, 5071-5080.

17 M. S. Spencer, *Top. Catal.*, 1999, **8**, 259-266.

18 L.-X. Zhang, Y.-C. Zhang, and S.-Y. Chen, *Appl. Catal. A: Gen.*, 2012, **415-416**, 118-123.

19 K. Klier, *Adv. Catal.*, 1982, **31**, 243-313.

20 F. Arena, G. Mezzatesta, G. Zafarana, G. Trunfio, F. Frusteri, and L. Spadaro, *J. Catal.*, 2013, **300**, 141-151.

21 L. Martínez-Suárez, J. Frenzel, D. Marx, and B. Meyer, *Phys. Rev. Lett.*, 2013, **110**, 086108.

22 S. Kühl, A. Tarasov, S. Zander, I. Kasatkin, and M. Behrens, *Chem. Eur. J.*, 2014, **20**, 3782-3792.

23 F. Wang, Y.-W. Liu, Y.-H. Gan, W. Ding, W.-P. Fang, and Y.-Q. Yang, *Fuel Process. Technol.*, 2013, **110**, 190-196.

24 J. Graciani, K. Mudiyanselage, F. Xu, A. E. Baber, J. Evans, S. D. Senanayake, D. J. Stacchiola, P. Liu, J. Hrbek, J. F. Sanz, and J. A. Rodriguez, *Science*, 2014, **345**, 546-550.

25 T. Witoon, T. Permsirivanich, W. Donphai, A. Jaree, and M. Chareonpanich, *Fuel Process. Technol.*, 2013, **116**, 72-78.

26 S. Natesakhawat, P. R. Ohodnicki, B. H. Howard, J. W. Lekse, J. P. Baltrus, and C. Matranga, *Top. Catal.*, 2013, **56**, 1752-1763.

27 V. Schott, H. Oberhofer, A. Birkner, M.-C. Xu, Y.-M. Wang, M. Muhler, K. Reuter, and C. Wöll, *Angew. Chem. Int. Ed.*, 2013, **52**, 11925-11929.

28 J. C. J. Bart and R. P. A. Sneeden, *Catal. Today*, 1987, **2**, 1-124.

29 Z.-S. Hong, Y. Cao, J.-F. Deng, and K.-N. Fan, *Catal. Lett.*, 2002, **82**, 37-44.

30 F. Arena, G. Italiano, K. Barbera, S. Bordiga, G. Bonura, L. Spadaro, and F. Frusteri, *Appl. Catal. A: Gen.*, 2008, **350**, 16-23.

31 S. Kuld, C. Conradsen, P. G. Moses, I. Chorkendorff, and J. Sehested, *Angew. Chem. Int. Ed.*, 2014, **53**, 5941-5945.

32 M. B. Fichtl, J. Schumann, I. Kasatkin, N. Jacobsen, M. Behrens, R. Schlögl, M. Muhler, and O. Hinrichsen, *Angew. Chem. Int. Ed.*, 2014, **53**, 7043-7047.

33 Q.-L. Tang, Q.-J. Hong, and Z.-P. Liu, *J. Catal.*, 2009, **263**, 114-122.

34 M. Behrens, F. Studt, I. Kasatkin, S. Kühl, M. Hävecker, F. Abild-Pedersen, S. Zander, F. Girgsdies, P. Kurr, B.-L. Kniep, M. Tovar, R. W. Fischer, J. K. Nørskov, and R. Schlögl, *Science*, 2012, **336**, 893-897.

35 G. C. Chinchen, P. J. Denny, J. R. Jennings, M. S. Spencer, and K. C. Waugh, *Appl. Catal.*, 1988, **36**, 1-65.

36 K. C. Waugh, *Catal. Lett.*, 1999, **58**, 163-165.

37 T. Fujitani and J. Nakamura, *Catal. Lett.*, 1999, **63**, 245-247.

38 Y. Borodko and G. A. Somorjai, *Appl. Catal. A: Gen.*, 1999, **186**, 355-362.

39 M. V. Twigg and M. S. Spencer, *Appl. Catal. A-Gen.*, 2001, **212**, 161-174.

40 K. Klier, V. Chatikavanij, R. G. Herman, and G. W. Simmons, *J. Catal.*, 1982, **74**, 343-360.

41 J. Szanyi and D. W. Goodman, *Catal. Lett.*, 1991, **10**, 383-390.

42 Y. Kanai, T. Watanabe, T. Fujitani, M. Saito, J. Nakamura, and T. Uchijima, *Catal. Lett.*, 1994, **27**, 67-78.

43 J. C. Frost, *Nature*, 1988, **334**, 577-580.

44 J. Nakamura, T. Uchijima, Y. Kanai, and T. Fujitani, *Catal. Today*, 1996, **28**, 223-230.

45 F. Arena, K. Barbera, G. Italiano, G. Bonura, L. Spadaro, and F. Frusteri, *J. Catal.*, 2007, **249**, 185-194.

46 J. Bao, Z.-L. Liu, Y. Zhang, and N. Tsubaki, *Catal. Commun.*, 2008, **9**, 913-918.

47 N. Park, M.-J. Park, Y.-J. Lee, K.-S. Ha, and K.-W. Junc, *Fuel Process. Technol.*, 2014, **125**, 139-147.

48 G. C. Chinchen, K. C. Waugh, and D. A. Whan, *Appl. Catal.*, 1986, **25**, 101-107.

49 W. X. Pan, R. Cao, D. L. Roberts, and G. L. Griffin, *J. Catal.*, 1988, **114**, 440-446.

50 R. Burch, S. E. Gohmski, and M. S. Spencer, *J. Chem. Soc., Faraday Trans.*, 1990, **86**, 2683-2691.

51 R. Burch, S. E. Golunski, and M. S. Spencer, *Catal. Lett.*, 1990, **5**, 55-60.

52 I. Chorkendorff, P. A. Taylor, and P. B. Rasmussen, *J. Vac. Sci. Technol. A*, 1992, **10**, 2277-2281.

53 P. B. Rasmussen, P. M. Holmblad, T. Askgaard, C. V. Ovesen, P. Stoltze, J. K. Norskov, and I. Chorkendorff, *Catal. Lett.*, 1994, **26**, 373-381.

54 P. B. Rasmussen, M. Kazuta, and I. Chorkendorff, *Surf. Sci.*, 1994, **318**, 267-280.

55 P. A. Taylor, P. B. Rasmussen, and I. Chorkendorff, *J. Chem. Soc., Faraday Trans.*, 1995, **91**, 1267-1269.

56 J. Yoshihara, S. C. Parker, A. Schafer, and C. T. Campbell, *Catal. Lett.*, 1995, **31**, 313-324.

57 J. Yoshihara and C. T. Campbell, *J. Catal.*, 1996, **161**, 776-782.

58 C. V. Ovesen, B. S. Clausen, J. Schiotz, P. Stoltze, H. Topsøe, and J. K. Nørskov, *J. Catal.*, 1997, **168**, 133-142.

59 K.-W. Jun, W.-J. Shen, K. S. R. Rao, and K.-W. Lee, *Appl. Catal. A: Gen.*, 1998,

174, 231-238.

60 C. Baltes, S. Vukojević, and F. Schüth, *J. Catal.*, 2008, **258**, 334-344.

61 H.-W. Lim, M.-J. Park, S.-H. Kang, H.-J. Chae, J. W. Bae, and K.-W. Jun, *Ind. Eng. Chem. Res.*, 2009, **48**, 10448-10455.

62 Y. Yang, C. A. Mims, R. S. Disselkamp, J.-H. Kwak, C. H. F. Peden, and C. T. Campbell, *J. Phys. Chem. C*, 2010, **114**, 17205-17211.

63 K. C. Waugh, *Catal. Today*, 1992, **15**, 51-75.

64 Q. Sun, Y.-L. Zhang, H.-Y. Chen, J.-F. Deng, D. Wu, and S.-Y. Chen, *J. Catal.*, 1997, **167**, 92-105.

65 F. Studt, F. Abild-Pedersen, J. B. Varley, and J. K. Nørskov, *Catal. Lett.*, 2013, **143**, 71-73.

66 S. Natesakhawat, J. W. Lekse, J. P. Baltrus, P. R. Ohodnicki, B. H. Howard, X.-Y. Deng, and C. Matranga, *ACS Catal.*, 2012, **2**, 1667-1676.

67 O. Martin and J. Pérez-Ramírez, *Catal. Sci. Technol.*, 2013, **3**, 3343-3352.

68 H. Jeong, C. H. Cho, and T. H. Kim, *Reac. Kinet. Mech. Cat.*, 2012, **106**, 435-443.

69 Y.-F. Zhao, Y. Yang, C. Mims, C. H. F. Peden, J. Li, and D.-H. Mei, *J. Catal.*, 2011, **281**, 199-211.

70 L. C. Grabow and M. Mavrikakis, *ACS Catal.*, 2011, **1**, 365-384.

71 O.-S. Joo, K.-D. Jung, S.-H. Han, S.-J. Uhm, D.-K. Lee, and S.-K. Ihm, *Appl. Catal. A: Gen.*, 1996, **135**, 273-286.

72 R. Burch, R. J. Chappell, and S. E. Golunski, *J. Chem. Soc., Faraday Trans. 1*, 1989, **85**, 3569-3578.

73 X. M. Guo, D. S. Mao, G. Z. Lu, S. Wang, and G. S. Wu, *Catal. Commun.*, 2011, **12**, 1095-1098.

74 T. Fujitani, I. Nakamura, T. Uchijima, and J. Nakamura, *Surf. Sci.*, 1997, **383**, 285-298.

75 T. Fujitani, T. Matsuda, Y. Kushida, S. Ogihara, T. Uchijima, and J. Nakamura, *Catal. Lett.*, 1997, **49**, 175-179.

76 T. Fujitani and J. Nakamura, *Catal. Lett.*, 1998, **56**, 119-124.

77 T. Fujitani and J. Nakamura, *Appl. Catal. A: Gen.*, 2000, **191**, 111-129.

78 Y. Choi, K. Futagami, T. Fujitani, and J. Nakamura, *Catal. Lett.*, 2001, **73**, 27-31.

79 J. Nakamura, Y. Choi, and T. Fujitani, *Top. Catal.*, 2003, **22**, 277-285.

80 Y. Sakata, M. A. Uddin, A. Muto, and M. Imaoka, *Microporous Mat.*, 1997, **9**,

183-187.

81 N.-Y. Topsøe and H. Topsøe, *Top. Catal.*, 1999, **8**, 267-270.

82 J. F. Edwards and G. L. Schrader, *J. Catal.*, 1985, **94**, 175-186.

83 G. H. Graaf, E. J. Stamhuis, and A. A. C. M. Beenackers, *Chem. Eng. Sci.*, 1988, **43**, 3185-3195.

84 T. Fujitani, I. Nakamura, T. Watanabe, T. Uchijima, and J. Nakamura, *Catal. Lett.*, 1995, **35**, 297-302.

85 S. A. French, A. A. Sokol, S. T. Bromley, C. R. A. Catlow, and P. Sherwood, *Top. Catal.*, 2003, **24**, 161-172.

86 M. Bowker, R. A. Hadden, H. Houghton, J. N. K. Hyland, and K. C. Waugh, *J. Catal.*, 1988, **109**, 263-273.

87 Z.-J. Zuo, P.-D. Han, Z. Li, J.-S. Hu, and W. Huang, *Appl. Surf. Sci.*, 2012, **261**, 640-646.

88 A. J. Medford, J. Sehested, J. Rossmeisl, I. Chorkendorff, F. Studt, J. K. Nørskov, and P. G. Moses, *J. Catal.*, 2014, **309**, 397-407.

89 G. Kresse and J. Hafner, *Phys. Rev. B*, 1993, **47**, 558-561.

90 G. Kresse and J. Hafner, *Phys. Rev. B*, 1993, **48**, 13115-13118.

91 G. Kresse and J. Hafner, *Phys. Rev. B*, 1994, **49**, 14251-14269.

92 G. Kresse and J. Furthmüller, *Comput. Mater. Sci.*, 1996, **6**, 15-50.

93 G. Kresse and J. Furthmüller, *Phys. Rev. B*, 1996, **54**, 11169-11186.

94 J. P. Perdew and Y. Wang, *Phys. Rev. B*, 1992, **45**, 13244-13249.

95 P. E. Blöchl, *Phys. Rev. B*, 1994, **50**, 17953-17979.

96 G. Kresse and D. Joubert, *Phys. Rev. B*, 1999, **59**, 1758-1775.

97 S. L. Dudarev, G. A. Botton, S. Y. Savrasov, C. J. Humphreys, and A. P. Sutton, *Phys. Rev. B*, 1998, **57**, 1505-1509.

98 P. Erhart, K. Albe, and A. Klein, *Phys. Rev. B*, 2006, **73**, 205203.

99 Q.-L. Tang and Q.-H. Luo, *J. Phys. Chem. C*, 2013, **117**, 22954-22966.

100 M. Methfessel and A. T. Paxton, *Phys. Rev. B*, 1989, **40**, 3616-3621.

101 P. Pulay, *Chem. Phys. Lett.*, 1980, **73**, 393-398.

102 B. Hammer, *Top. Catal.*, 2006, **37**, 3-16.

103 U. Diebold, L. V. Koplitz, and O. Dulub, *Appl. Surf. Sci.*, 2004, **237**, 336-342.

104 J. Wróbel and J. Piechota, *Solid Stat. Comm.*, 2008, **146**, 324-329.

105 Y. Azzaz, S. Kacimi, A. Zaoui, and B. Bouhafs, *Physica B*, 2008, **403**, 3154-3158.

106 B. Meyer and D. Marx, *Phys. Rev. B*, 2003, **67**, 035403.

107 J. Hu, W.-P. Guo, X.-R. Shi, B.-R. Li, and J.-G. Wang, *J. Phys. Chem. C*, 2009, **113**, 7227-7235.

108 P. L. Hansen, J. B. Wagner, S. Helveg, J. R. Rostrup-Nielsen, B. S. Clausen, and H. Topsøe, *Science*, 2002, **295**, 2053-2055.

109 M. Sano, T. Adaniya, T. Fujitani, and J. Nakamura, *Surf. Sci.*, 2002, **514**, 261-266.

110 J. A. Rodriguez, P. Liu, J. Hrbek, J. Evans, and M. Pérez, *Angew. Chem. Int. Ed.*, 2007, **46**, 1329-1332.

111 Q.-L. Tang and Z.-P. Liu, *J. Phys. Chem. C*, 2010, **114**, 8423-8430.

112 C.-M. Wang, K.-N. Fan, and Z.-P. Liu, *J. Am. Chem. Soc.*, 2007, **129**, 2642-2647.

113 Z.-P. Liu, X.-Q. Gong, J. Kohanoff, C. Sanchez, and P. Hu, *Phys. Rev. Lett.*, 2003, **91**, 266102.

114 Z.-P. Liu, S. J. Jenkins, and D. A. King, *Phys. Rev. Lett.*, 2004, **93**, 156102.

115 H. J. Monkhorst and J. D. Pack, *Phys. Rev. B*, 1976, **13**, 5188-5192.

116 G. Mills, H. Jónsson, and G. K. Schenter, *Surf. Sci.*, 1995, **324**, 305-337.

117 G. Henkelman, B. P. Uberuaga, and H. Jónsson, *J. Chem. Phys.*, 2000, **113**, 9901-9904.

118 Q.-L. Tang, S.-R. Zhang, and Y.-P. Liang, *J. Phys. Chem. C*, 2012, **116**, 20321-20331.

119 W. F. K. Wynne-Jones and H. Eyring, *J. Chem. Phys.*, 1935, **3**, 492-502.

120 I. Chorkendorff, J.W. Niemantsverdriet, *Concepts of Modern Catalysis and Kinetics*, Wiley-VCH Verlag GmbH & Co. KGaA, Weinheim, 2003.

121 Q.-L. Tang, *Int. J. Quantum Chem.*, 2013, **113**, 1992-2001.

122 M. Muhler, L. P. Nielsen, E. Törnqvist, B. S. Clausen, and H. Topsøe, *Catal. Lett.*, 1992, **14**, 241-249.

123 J. P. Perdew, K. Burke, and M. Ernzerhof, *Phys. Rev. Lett.*, 1996, **77**, 3865-3868.

124 M. Hellström, D. Spångberg, K. Hermansson, and P. Broqvist, *Phys. Rev. B*, 2012, **86**, 235302.

125 A. Rohrbach, J. Hafner, and G. Kresse, *Phys. Rev. B*, 2004, **69**, 075413.

126 A. Rohrbach and J. Hafner, *Phys. Rev. B*, 2005, **71**, 045405.

127 D. R. Alfonso, J. E. Jaffe, A. C. Hess, and M. Gutowski, *Phys. Rev. B*, 2003, **68**, 155411.

128 R. F. W. Bader, *Accounts Chem. Res.*, 1985, **18**, 9-15.

129 G. Henkelman, A. Arnaldsson, and H. Jónsson, *Comput. Mater. Sci.*, 2006, **36**, 354-360.

130 B. Meyer, *Phys. Rev. B*, 2004, **69**, 045416.

131 Y. Kanai, T. Watanabe, T. Fujitani, T. Uchijima, and J. Nakamura, *Catal. Lett.*, 1996, **38**, 157-163

132 N.-Y. Topsøe and H. Topsøe, *J. Mol. Catal. A: Chem.*, 1999, **141**, 95-105.

133 D.R. Lide, *CRC Handbook of Chemistry and Physics*, 84th ed., CRC Press, Boca Raton, FL, 2003-2004, pp. 5-1 and 5-2.

134 *http://webbook.nist.gov/*.

135 D. Bianchi, J.-L. Gass, M. Khalfallah, and S. J. Teichner, *Appl. Catal. A: Gen.*, 1993, **101**, 297-315.

136 G. Ertl, *Surf. Sci.*, 1994, **299/300**, 742-754.

137 A. J. Elliott, M. J. Watson, J. Tabatabaei, F. W. Zemichael, and K. C. Waugh, *Catal. Lett.*, 2002, **79**, 1-6.

138 C. Schild, A. Wokaun, and A. Baiker, *J. Mol. Catal.*, 1990, **63**, 243-254.

139 I. A. Fisher and A. T. Bell, *J. Catal.*, 1997, **172**, 222-237.

140 J. N. Brönsted, *Chem. Rev.*, 1928, **5**, 231-338.

141 M. G. Evans and M. Polanyi, *Trans. Faraday Soc.*, 1936, **32**, 1333-1360.

Table 1 Preferred adsorption sites[a], binding energies (E_{ad}, eV) and adsorbate (A)-substrate (Cu) bond lengths ($d_{A\text{-}Cu}$, Å) of intermediates relevant to methanol synthesis from CO_2 hydrogenation, calculated on the Cu side of the Cu/ZnO interface boundary[b]

Species	Site	E_{ad}	$E_{ad}^{Cu(111)}$	$E_{ad}-E_{ad}^{Cu(111)}$	A-Cu	$d_{A\text{-}Cu}$
H	Phcp	-2.80	-2.51	-0.29	H-Cu	1.70/1.71/1.72
O	Phcp	-5.01	-4.69	-0.32	O-Cu	1.87/1.87/1.92
H_2	Atop1	-0.10	-0.01	-0.09	H-Cu	1.80
OH	Phcp	-3.24	-3.07	-0.17	O-Cu	1.97/2.01/2.04
CO	Phcp	-1.22	-0.86	-0.36	C-Cu	2.00/2.00/2.01
H_2O	Atop1	-0.34	-0.21	-0.13	O-Cu	2.19
CO_2	Atop1	-0.06	-0.05	-0.01	O-Cu	3.27
COH	Phcp	-3.38	-2.78	-0.60	C-Cu	1.90/1.91/1.96
HCO	Bri3–Atop1	-1.77	-1.30	-0.47	C-Cu	2.02/2.04
					O-Cu	2.09
mono-HCOO	Phcp	-2.47	-2.28	-0.19	O-Cu	2.03/2.08/2.13
bi-HCOO	Atop1– Atop1	-3.23	-2.85	-0.38	O-Cu	1.97/1.98
trans-HOCO	Atop2– Atop1	-1.89	-1.64	-0.25	C-Cu	1.93
					O-Cu	2.06
cis-HOCO	Atop2– Atop1	-1.92	-1.66	-0.26	C-Cu	1.93
					O-Cu	2.06
H_2CO	Atop1– Atop1	-0.38	-0.11	-0.27	C-Cu	2.17
					O-Cu	1.95
HCOH	Pfcc	-2.30	-1.94	-0.36	C-Cu	2.04/2.06/2.08
H_3CO	Phcp	-2.50	-2.35	-0.15	O-Cu	1.98/2.02/2.05
H_2COH	Bri3	-1.44	-1.05	-0.39	C-Cu	2.09/2.18
H_2COO	Bri1-Bri3	-4.45	-4.07	-0.38	O-Cu	1.95/1.96/1.99/2.01
HCOOH	Atop1	-0.51	-0.24	-0.27	O-Cu	2.09
HOCOH	Atop1	-1.54	-1.37	-0.17	C-Cu	1.90
H_3COH	Atop1	-0.36	-0.19	-0.17	O-Cu	2.14
H_2COOH	Atop2-Bri1	-2.39	-2.12	-0.27	O-Cu	2.00/2.01/2.19

[a]For hollow site adsorption, the phcp and pfcc configurations are nearly degenerate

with an energy difference of typically < 0.05 eV. See Fig. 1 for site nomenclature.

[b]Also shown are adsorption energies, $E_{\mathrm{ad}}^{\mathrm{Cu(111)}}$, for the most stable states of the various binding complexes on Cu(111) as a reference metallic surface. Distances of the bonds within the diatomic and polyatomic adsorbates at the materials' interface are given in Fig. 2.

Table 2 Thermochemical and kinetic parameters computed for the elementary steps (ES) involved in CO_2 hydrogenation to methanol at the Cu site of the Cu/ZnO interface[a]

ES No.	ES	ν^{img}	E_r	E_a	A^0	k	k_r
1	$H_2 + 2* \rightarrow 2H*$	519i	-1.00	0.23	$6.50 \times 10^{7\,b}$	3.95×10^{5}	1.61×10^{2}
2	$CO_2 + H* \rightarrow$ mono-HCOO*	537i	0.49	0.79	$1.07 \times 10^{6\,b}$	2.62×10^{-2}	4.81×10^{9}
3	mono-HCOO* $\rightarrow$ bi-HCOO*	79i	-0.80	0.10	1.40×10^{12}	1.52×10^{11}	1.23×10^{4}
4	bi-HCOO* + H* $\rightarrow H_2COO* + *$	619i	1.26	2.10	4.11×10^{12}	2.38×10^{-8}	4.90×10^{5}
5	$H_2COO* + H* \rightarrow H_2COOH* + *$	343i	0.19	1.22	1.12×10^{13}	1.96×10^{1}	3.15×10^{2}
6	bi-HCOO* + H* $\rightarrow$ HCOOH* + *	1031i	0.85	1.10	1.28×10^{13}	3.21×10^{2}	9.73×10^{10}
7	HCOOH* + H* $\rightarrow H_2COOH* + *$	836i	0.60	1.29	1.71×10^{14}	6.34×10^{1}	2.80×10^{7}
8	$H_2COOH* + * \rightarrow H_2CO*\cdots OH*$	53i	0.27	0.28	6.78×10^{12}	1.36×10^{10}	3.81×10^{11}
9	$H_2CO* + H* \rightarrow H_3CO* + *$	860i	-0.35	0.48	1.84×10^{13}	4.36×10^{8}	9.81×10^{4}
10	$H_3CO* + H* \rightarrow H_3COH* + *$	1232i	0.38	1.34	5.84×10^{13}	7.14×10^{0}	3.31×10^{3}
11	$OH* + H* \rightarrow H_2O* + *$	983i	0.38	1.28	2.53×10^{13}	1.17×10^{1}	5.57×10^{3}
12	$H_3CO* + H_2O* \rightarrow H_3COH* + OH*$	81i	0.02	0.02	3.32×10^{13}	2.13×10^{13}	1.35×10^{13}
13	$CO_2 + H* \rightarrow$ *trans*-HOCO*	1338i	0.70	1.43	$5.50 \times 10^{5\,b}$	9.13×10^{-9}	1.80×10^{6}
14	$CO_2 + H_2O* + * \rightarrow$ *trans*-HOCO*$\cdots$OH*	379i	0.24	0.27	$1.07 \times 10^{4\,b}$	3.07×10^{2}	5.12×10^{12}
15	*trans*-HOCO* $\rightarrow$ *cis*-HOCO*	614i	-0.04	0.40	2.42×10^{13}	3.38×10^{9}	1.48×10^{9}
16	*cis*-HOCO* + H* $\rightarrow$ HOCOH* + *	1232i	0.79	1.07	1.78×10^{13}	8.68×10^{2}	8.47×10^{10}
17	*cis*-HOCO* + H* $\rightarrow$ HCOOH* + *	797i	-0.06	0.97	1.62×10^{13}	7.30×10^{3}	8.41×10^{2}
18	HOCOH* +* $\rightarrow$ COH* + OH*	309i	0.06	1.29	7.23×10^{13}	2.68×10^{1}	2.12×10^{1}
19	COH* + H* $\rightarrow$ HCOH* + *	638i	0.41	1.02	1.89×10^{13}	2.81×10^{3}	6.84×10^{6}
20	HCOH* + H* $\rightarrow H_2COH* + *$	570i	-0.07	0.87	1.55×10^{13}	6.43×10^{4}	2.07×10^{4}
21	$H_2COH* + H* \rightarrow H_3COH* + *$	867i	-0.28	0.85	1.33×10^{13}	8.59×10^{4}	1.26×10^{1}
22	$CO_2 + 2* \rightarrow CO* + O*$	266i	0.12	1.00	$1.37 \times 10^{6\,b}$	8.36×10^{-5}	1.91×10^{1}
23	*cis*-HOCO* + * $\rightarrow$ CO* + OH*	278i	-0.61	0.44	2.05×10^{13}	1.18×10^{9}	6.31×10^{2}
24	CO* + H* $\rightarrow$ COH* + *	1597i	1.45	2.17	8.52×10^{12}	1.05×10^{-8}	9.07×10^{5}
25	CO* + H* $\rightarrow$ HCO* + *	736i	1.17	1.44	2.37×10^{13}	3.15×10^{-1}	3.03×10^{10}
26	HCO* + H* $\rightarrow H_2CO* + *$	979i	0.31	0.84	1.15×10^{13}	9.24×10^{4}	3.35×10^{6}
27	O* + H* $\rightarrow$ OH* + *	927i	-0.07	1.08	1.36×10^{13}	5.32×10^{2}	3.66×10^{1}
28	2OH* $\rightarrow H_2O*\cdots O*$	407i	0.14	0.26	9.77×10^{12}	3.05×10^{10}	1.14×10^{12}

29	$HCOOH^* \rightarrow HCOOH + *$	-	0.51	0.51	1.09×10^{13}	1.33×10^{8}	3.06×10^{-2}
30	$H_2CO^{*}\cdots OH^* \rightarrow H_2CO^* + OH^*$	-	0.07	0.07	1.09×10^{13}	2.31×10^{12}	1.09×10^{13}
31	$H_2CO^* \rightarrow H_2CO + *$	-	0.38	0.38	1.09×10^{13}	2.37×10^{9}	1.66×10^{0}
32	$H_3COH^* \rightarrow H_3COH + *$	-	0.36	0.36	1.09×10^{13}	3.70×10^{9}	9.29×10^{-2}
33	*trans*-$HOCO^{*}\cdots OH^* \rightarrow$ *trans*-$HOCO^* + OH^*$	-	0.10	0.10	1.09×10^{13}	1.18×10^{12}	1.09×10^{13}
34	$CO^* \rightarrow CO + *$	-	1.22	1.22	1.09×10^{13}	1.91×10^{1}	7.23×10^{1}
35	$H_2O^{*}\cdots O^* \rightarrow H_2O^* + O^*$	-	0.28	0.28	1.09×10^{13}	2.18×10^{10}	1.09×10^{13}
36	$H_2O^* \rightarrow H_2O + *$	-	0.34	0.34	1.09×10^{13}	5.77×10^{9}	1.41×10^{2}
37[c]	$H^* + *' \rightarrow H*' + *$	393i	0.29	0.42	1.09×10^{13}	9.77×10^{8}	6.09×10^{11}
38[c]	$H^* + *'' \rightarrow H*'' + *$	707i	0.25	1.18	1.09×10^{13}	4.64×10^{1}	1.19×10^{4}

[a] ν^{img} (cm^{-1}), only imaginary mode at the TS; E_r (eV), heat of reaction corrected for vibrational energies; E_a (eV), vibrational-energy corrected activation energy; A^0 (s^{-1}), preexponential factor; k (s^{-1}), reaction rate constant; k_r (s^{-1}), reverse rate constant. The values of E_r and E_a for a specific surface reaction are referenced to the reactants and/or products adsorbed at infinite separation on the phase boundary. The vibrational energy, including both all zero-point energies and temperature contribution, was calculated according to eqn (2) of ref. 118. A negative E_r value means that the reaction releases energy. * denotes a vacant interfacial site. For surface bound states X* + Y* and X*···Y*, the X* and Y* species are separately adsorbed and coadsorbated on the slab, respectively. In typical methanol production conditions with a total pressure of 5 MPa and 523 K, we set the feed composition as 25% CO_2 and 75% H_2 similar to the composition in the study of Nakamura and co-workers (from ref. 44); see also section 2.

[b] In the case of ER mechanism reactions, low A^0 values are owing primarily to a large entropy of the gas-phase H_2 or CO_2 molecule at the studied temperature.

[c] The hopping of adsorbed atomic H occurs from the boundary site to the bulk Cu(111) facet (*′) and simultaneously to the ZnO support (*″).

Table 3 Surface coverages (θ, ML) of adsorbates at steady state predicted for CO_2 hydrogenation to methanol on the Cu side of the Cu/ZnO interface[a].

Species	θ		Species	θ
H*	9.96×10^{-1}		H_2CO*	4.56×10^{-18}
O*	3.81×10^{-11}		HCOH*	1.06×10^{-23}
OH*	1.62×10^{-10}		H_3CO*	1.17×10^{-12}
CO*	1.90×10^{-10}		H_2COH*	7.89×10^{-24}
H_2O*	3.33×10^{-19}		H_2COO*	2.58×10^{-15}
COH*	3.38×10^{-22}		HCOOH*	1.96×10^{-10}
HCO*	5.52×10^{-19}		HOCOH*	6.01×10^{-20}
mono-HCOO*	2.50×10^{-11}		H_3COH*	2.25×10^{-21}
bi-HCOO*	2.95×10^{-4}		H_2COOH*	2.97×10^{-16}
trans-HOCO*	9.23×10^{-15}		*	3.57×10^{-3}
cis-HOCO*	2.10×10^{-14}			

[a]All 38 elementary steps shown in Table 2 were included in the microkinetic model. For the reaction conditions used, see footnote *a* to that table.

Table 4 Calculated turnover frequencies (TOFs, s^{-1}) of CO_2 hydrogenation at the Cu site of the Cu/ZnO interface[a].

TOF				
CO	H_2CO	HCOOH	H_3COH	H_2O
3.05×10^{-13}	9.72×10^{-13}	3.60×10^{-6}	8.01×10^{-16}	1.04×10^{-13}

[a]See footnote *a* to Table 2 for the reaction conditions adopted.

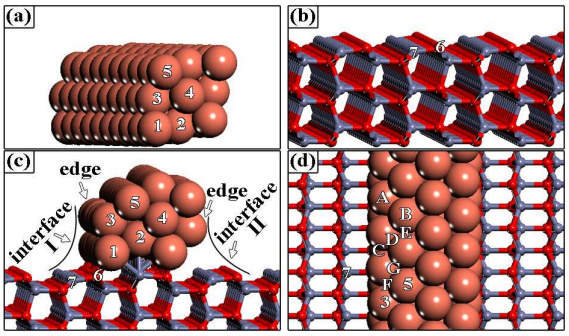

Fig. 1 Lateral views of an isolated Cu strip (a) and a clean $(10\bar{1}0)$ facet of ZnO (b), and side (c) and top views (d), respectively, of the optimized structure after deposition of (a) on (b), namely the Cu/ZnO model system employed in this work. In Plot c, the two formed complementary Cu–ZnO interfaces (I and II) are highlighted with arrows. All the interfacial adsorption/reaction sites under scrutiny are located directly at the edge-Cu atoms of interface I or in their immediate vicinity (see text for detailed interpretation), as labeled with the letters in Plot d as follows: A, edge-atop (termed Atop1); B, terrace-atop (Atop2); C-E, three kinds of bridges (abbreviated as bri1, bri2 and bri3, respectively); F, pseudo-fcc 3-fold hollow (pfcc); G, pseudo-hcp 3-fold hollow (phcp). The pfcc and phcp locations evolved, respectively, from the hcp and fcc counterparts of the unrelaxed strip surface. Numbers identify the relevant atomic rows. Small red balls, lattice O; large orange balls, Cu; small blue balls, Zn. This notation was applied throughout the article.

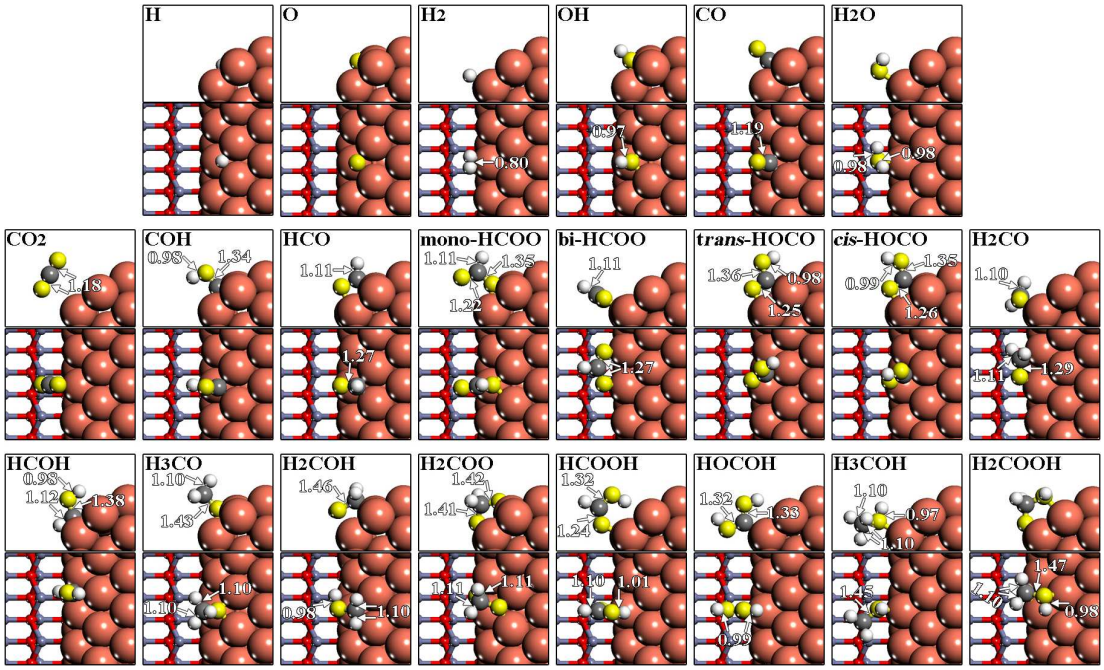

Fig. 2 Most stable binding configurations for all the possible intermediates implicated in methanol synthesis through CO_2 hydrogenation over the copper phase of the Cu/ZnO interface. Upper and lower panels of each pair of images provide a cross section and a top view of the separately adsorbed species, respectively. The internal bond lengths for adsorbates are given in units of Å. Atomic spheres: white, H; gray, C; yellow, adsorbate O. This notation was used throughout the paper.

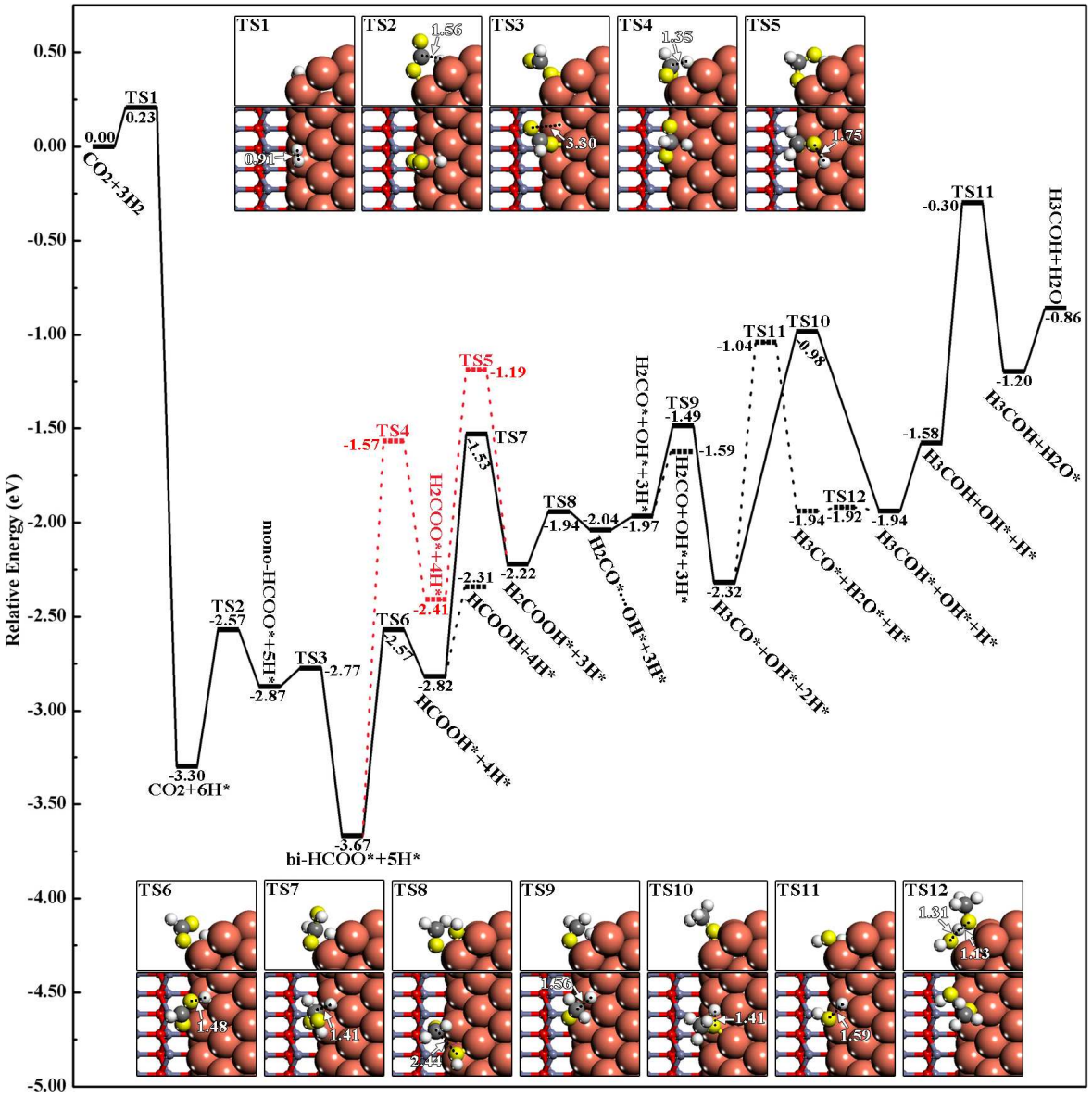

Fig. 3 Potential energy diagram for CO_2 hydrogenation leading to methanol at the Cu side of the Cu/ZnO interface via the HCOO path. The reaction mechanism diverges at the point of bi-HCOO* to include the novel isomeric complexes H_2COO* and HCOOH*. The electronic energy was corrected for contributions from vibration energies at 523 K. The zero energy is taken as the sum of the energies of the bare Cu/ZnO system, gaseous carbon dioxide, and gaseous molecular hydrogen. "TSi" stands for the transition state of the i-th elementary reaction listed in Table 2. Inserts provide side (upper panels) and top views (lower panels) of each calculated TS structure. Selected breaking and/or forming bond distances, as marked by arrows, are shown in Å. The equilibrium geometries of adsorbed intermediates at infinite

separation from each other on the slab are illustrated in Fig. 2. The same representations were used in subsequent figures.

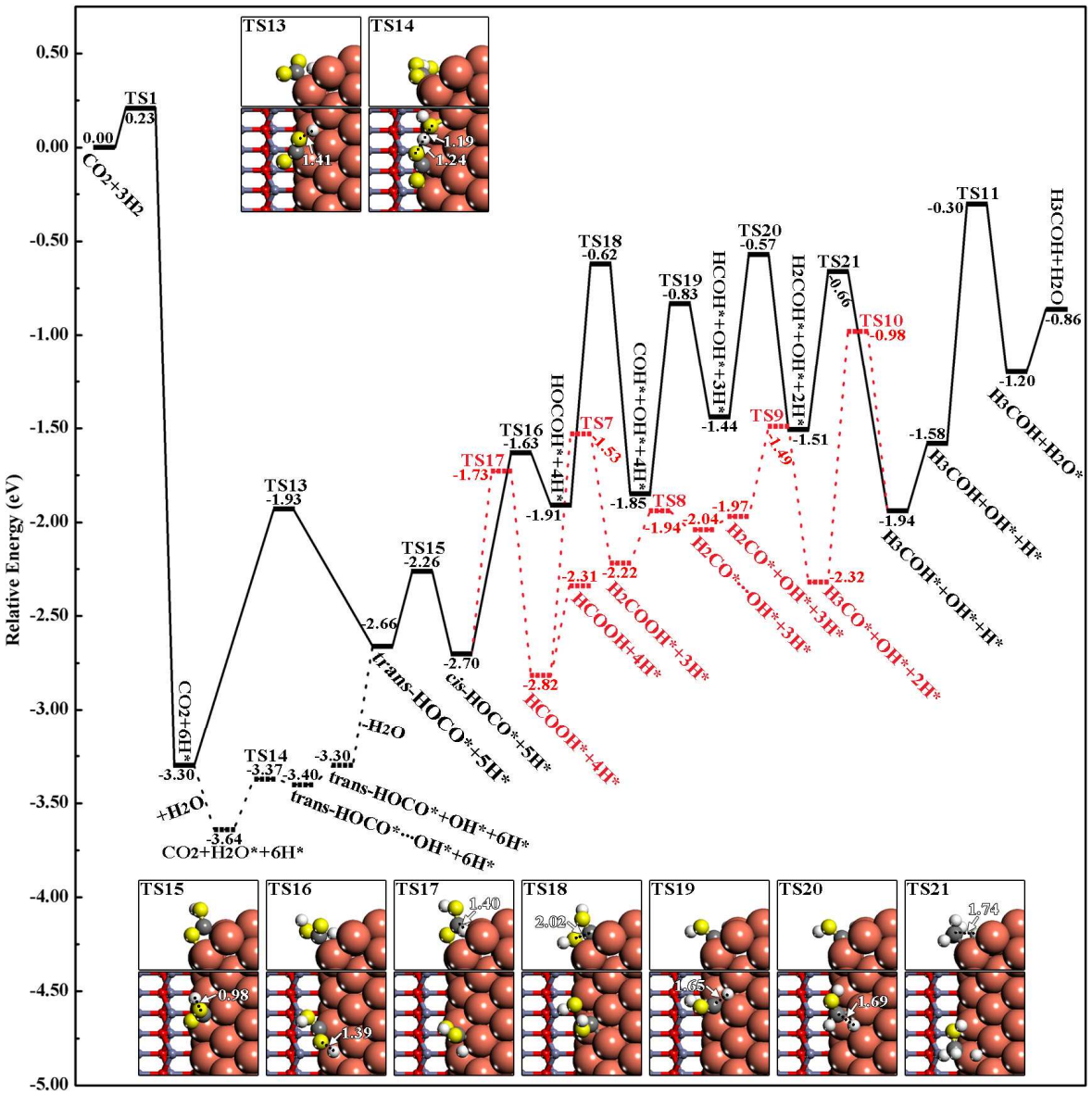

Fig. 4 Reaction coordinate for CO_2 hydrogenation to give methanol at the Cu site of the Cu/ZnO boundary along the HOCO path. The reaction route is bifurcated from *cis*-HOCO*. The TS structures not displayed here are available in Fig. 3.

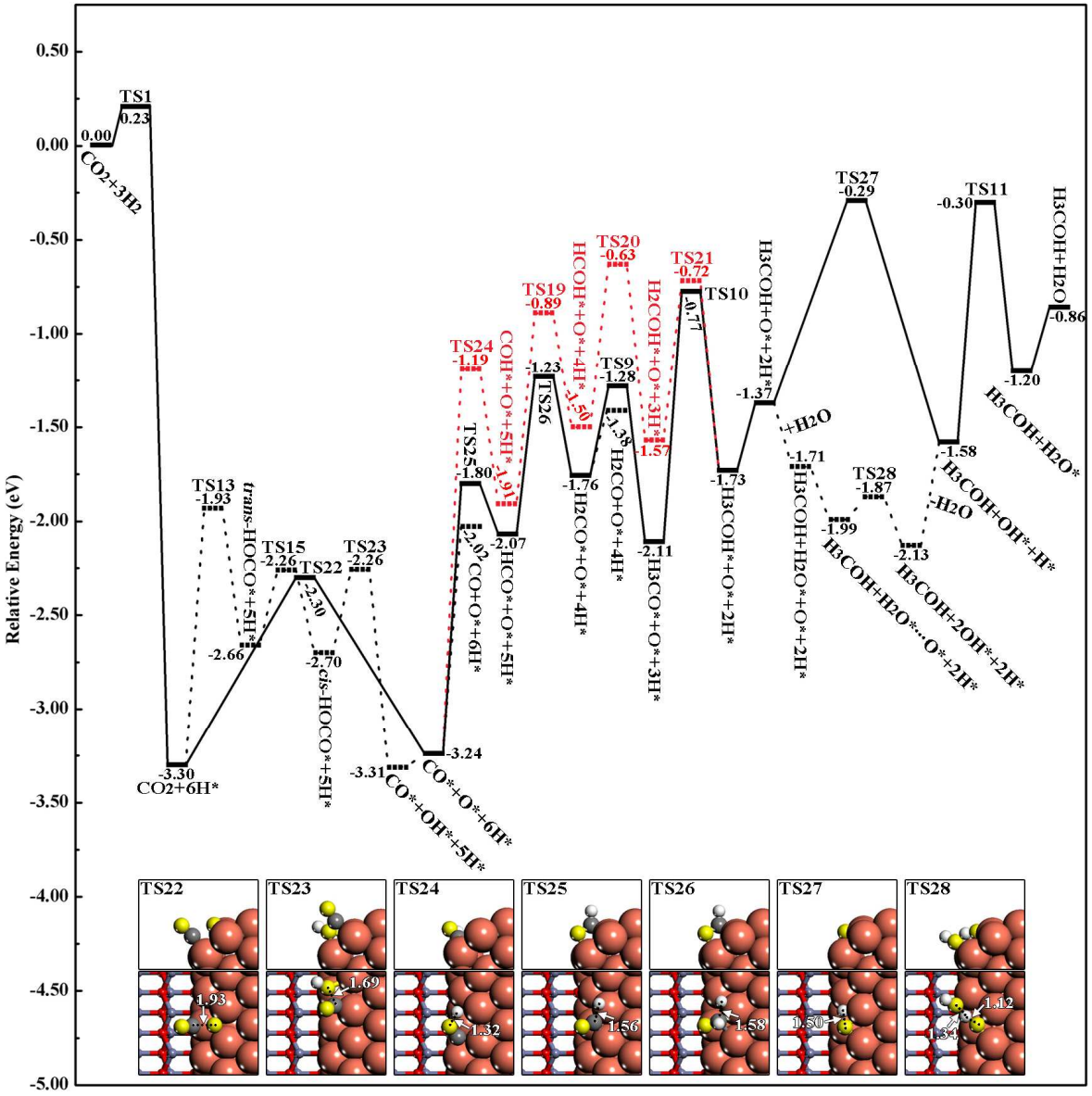

Fig. 5 Energy profile of methanol formation from CO_2 and H_2 on the Cu side of the Cu/ZnO interface through the CO path. Here, two parallel hydrogenation branches involving COH* and HCO* were taken into account. The TS structures not shown in this figure were already given in Fig. 3 or 4.